Chemical and Structural Evolution of Rb 2–2 x K 2 x Ti 2 O 5 Layered Titanates When Exposed to Ambient Air

Narimane Meziani, Méline Parent, Gwenaëlle Rousse, Brigitte C. Leridon, David Berardan, Paola Giura

Accepted for publication in Inorganic Chemistry, https://doi.org/10.1021/acs.inorgchem.4c02003

Chemical and structural evolution of $Rb_{2-2x}K_{2x}Ti_2O_5$ layered titanates when exposed to ambient air

Narimane Meziani[1], Méline Parent[2], Gwenaëlle Rousse[3], Brigitte Leridon[4], David Berardan[1,*], Paola Giura[2,*]

1. Institut de Chimie Moléculaire et des Matériaux d'Orsay, CNRS, Université Paris-Saclay, Orsay, France

2. Institut de Minéralogie, de Physique des Matériaux et de Cosmochimie, Sorbonne Université, Paris, France

3. Laboratoire de Chimie du Solide et Énergie, UMR 8260 , Collège de France, Sorbonne Université, Paris, France

4. Laboratoire de Physique et d'Etude des Matériaux, UMR8213 ESPCI Paris, PSL Université, CNRS, Sorbonne Université, Paris, France

*: corresponding authors

e-mail address: david.berardan@u-psud.fr paola.giura@sorbonne-universite.fr

Abstract

In this report, we combine thermogravimetric analysis, X-ray diffraction and infrared spectroscopy to investigate the chemical and structural evolution when exposed to ambient atmosphere of alkali titanates $Rb_2Ti_2O_5$, $K_2Ti_2O_5$, and mixed compound $Rb_{2-2x}K_{2x}Ti_2O_5$, with $0 \leq x \leq 1$. We show that a complete solid solution exists between the potassium and rubidium end-members and that mixed compounds exhibit an intermediate behavior. When exposed to the ambient atmosphere, all compounds degrade, with the progressive formation of first hydrates and then bicarbonates and a much quicker degradation of the rubidium titanate as compared to the potassium one. Reversely, we show that when hydrated in the absence of CO_2, the crystal structure of $K_2Ti_2O_5$ is more quickly impacted than that of $Rb_2Ti_2O_5$. These observations should be useful to understand the evolution of the functional properties of $M_2Ti_2O_5$ alkali titanates upon ageing in ambient atmosphere, as well as for the optimization of their hydration-dependent properties.

Introduction

Alkali titanates $M_2O.nTiO_2$ (M = alkali element) with layered or tunnel structures have been studied for a wide variety of potential applications depending on the value of the integer *n*. For example, $K_2Ti_6O_{13}$ and $K_2Ti_8O_{17}$ (M = K and *n* = 6 and 8) are used industrially as reinforcement materials. Among these materials, $M_2Ti_2O_5$ compounds with *n* = 2 have been less studied due to stability issues. They crystallize in a monoclinic structure, with alternate layers of Ti-O and M atoms stacked along the c-axis. Ti atoms present an unusual 5-fold coordination which is a square based pyramid. These TiO_5 polyedra share edges to form square-based pyramids double chains, with pyramid apexes pointing alternatively upwards and downwards. These chains share corners to form Ti-O layers in between which the alkali ions sit and is eightfold coordinated (Figure 1a)[1–3]. They have been studied with M = K for various functional properties and applications, including humidity sensors[4], NOx storage and reduction[5], anode materials for potassium-ion-batteries[6], electrode for capacitive deionization of ammonium[7], CO_2 capture at high temperature[8] or catalytic oxidation of carbon black[9], among other. Recently, $M_2Ti_2O_5$ with M = K or Rb have been suggested as promising supercapacitor electrolytes due to their colossal equivalent dielectric constant[10,11] and the formation of an unusual "virtual cathode" upon polarization[12]. It was further shown that these dielectric properties are strongly influenced by the exposure of the samples to the ambient atmosphere, which was attributed to the incorporation of water in the structure[13], although the study of the interactions between the compounds and the surrounding atmosphere remained preliminary. This sensitivity to water was independently confirmed by Chen *et al.* who evidenced a decrease of impedance at 10 kHz by a factor of circa 70 000 when increasing the humidity rate in the atmosphere surrounding $K_2Ti_2O_5$ from 11% to 94% using in-situ electrochemical impedance spectroscopy measurements[14]. However, these authors did not quantify the actual amount of water adsorbed on (or incorporated in) the materials, although they report that the impedance at a given humidity rate did not change after 9 days, which at a first glance seems to evidence that ageing did not influence the properties and that the samples did not degrade[14].
To date, although their knowledge would be of great importance to optimize the properties of $M_2Ti_2O_5$ for applications, understand their ageing, or even simply assess their real potential for long term applications, the studies of the reactions occurring when they are exposed to the ambient atmosphere remain non-existent. The only exception is a very preliminary study by Bamberger *et al*. who showed that the peaks of crystalline $K_2Ti_2O_5$ remained present in the Raman spectrum after exposure to ambient air during several days beside unidentified supplementary small peaks[15]. In this work, we use a combination of thermogravimetric analysis, infrared spectroscopy and X-ray diffraction to shed more light on the nature and the kinetic of the reactions that occur between $M_2Ti_2O_5$ (M = K, Rb) powder and the atmosphere, as well as the behavior of the $Rb_{2-2x}K_{2x}Ti_2O_5$ that is reported here for the first time.

Experimental section

$M_2Ti_2O_5$ (M=K, Rb) compounds were prepared through a standard solid-state synthesis route. Starting powders, titanium dioxide (TiO_2, Alfa 99.8%), and carbonates containing the alkali element (K_2CO_3, ThermoScientific, 99.997% and Rb_2CO_3, ThermoScientific, 99.98%), kept in glovebox to avoid hydration, were mixed in stoichiometric proportions. Then, the mixtures were compacted into rectangular bars (12mm× 3mm× 6mm) under a pressure of 300 MPa at room temperature. These bars were then annealed in an alumina crucible for 24 hours in ambient air at a specific temperature as

detailed in Table 1. The resulting samples were taken out of the furnace at 300°C and immediately transferred into the glovebox to minimize any possible interaction with the ambient atmosphere. Then the bars were grounded with an agate pestle and mortar in the glovebox and stored in powder form. All the samples used here to study the degradation of $M_2Ti_2O_2$ compounds are powders with similar particles size, in the range of few micrometers. Therefore, although the microstructure of the samples may obviously influence the kinetics of reaction with their surrounding environments, we can confidently infer that the different behaviors observed in this study are actually related to the nature of the alkali element.

Caution! Rubidium carbonate and potassium carbonate cause skin irritation, serious eye irritation and may cause respiratory irritation; they must be handled with care.

Compound	Stoichiometry of the precursors (K_2CO_3 : Rb_2CO_3 : TiO_2)	Synthesis temperature (°C)
$K_2Ti_2O_5$	(1 : 0: 2)	900
$K_{1.6}Rb_{0.4}Ti_2O_5$	(0.8: 0.2: 2)	870
$K_{1.2}Rb_{0.8}Ti_2O_5$	(0.4 : 0.6: 2)	870
$KRbTi_2O_5$	(1 : 1 : 2)	850
$K_{0.8}Rb_{1.2}Ti_2O_5$	(0.6: 0.4: 2)	830
$K_{0.4}Rb_{1.6}Ti_2O_5$	(0.2 : 0.8: 2)	830
$Rb_2Ti_2O_5$	(0: 1: 2)	800

Table 1: synthesis temperature of $Rb_{2-2x}K_{2x}Ti_2O_5$ samples.

The degradation of the as-synthesized samples was studied in two different ways. The first consisted of spreading as-synthesized $Rb_{2-2x}K_{2x}Ti_2O_5$ powders on a glass slide exposed to ambient air (temperature 20-25°C, relative humidity ≈25%) over different durations. The second method involved hydrating the $Rb_{2-2x}K_{2x}Ti_2O_5$ powders in a CO_2-free water-saturated atmosphere, using a configuration of glass vials nested in an argon atmosphere. One vial contained 0.4 ml of freshly distilled water introduced via a syringe, for every 300 mg of $Rb_{2-2x}K_{2x}Ti_2O_5$ powder, while the other vial contained the powdered compound.

The structures of the different compounds were studied by powder X-ray diffraction (XRD), using a PANalytical X'Pert diffractometer equipped with a Ge (111) monochromator and a Pixel detector, employing Cu $K\alpha_1$ radiation (λ=1.5406 Å). All measurements were performed in a closed chamber under argon using a sample holder equipped with a polycarbonate dome. Therefore, no evolution of

the samples is assumed to occur during the acquisition time. Then, structural parameters were determined by using the Le Bail refinement method with the help of FullProf software[16].

Thermogravimetric analysis (TGA) were performed using a Setaram Setsys Evo thermogravimetric analyser with alumina crucibles. The measurements were carried out under controlled atmosphere (O_2 with gas flow of 30 ml/min) up-to temperatures slightly below or equal to those of the syntheses, with a heating rate of 10 K/min. Before measuring each sample, an empty crucible was measured using the same conditions as the sample as a blank. If not specified otherway, all TGA data presented in the manuscript are subtracted from the blank. Typical masses of powders used for the analysis were of the order of 150 mg.

Mid-infrared spectroscopy measurements were performed using two different spectrometers. Those shown as a function of temperature were acquired in the wavenumber region (580 - 4000) cm^{-1} with a Bruker IFS66vs spectrometer equipped with a Janis helium flux cryo furnace operating between 10 and 700 K, a nitrogen cooled MCT detector, a KBr beamsplitter and a globar source. The measurements shown only at ambient temperature were performed using a Bruker ALPHA spectrometer operating in the wavenumber range (380-4000) cm^{-1}, in transmission geometry and equipped with a Deuterated TriGlycine Sulfate (DTGS) detector, a KBr beamsplitter and a globar source. Samples were prepared in pellets of 13mm in diameter, containing a molar fraction of 1% of the sample and 99% of KBr, directly in the glovebox by applying a pressure of 520 MPa at room temperature. Reference spectra were obtained by using a 100% KBr pellet measured in the same conditions as the samples. All infrared spectra presented in the manuscript are corrected from the KBr reference.

Results and discussions

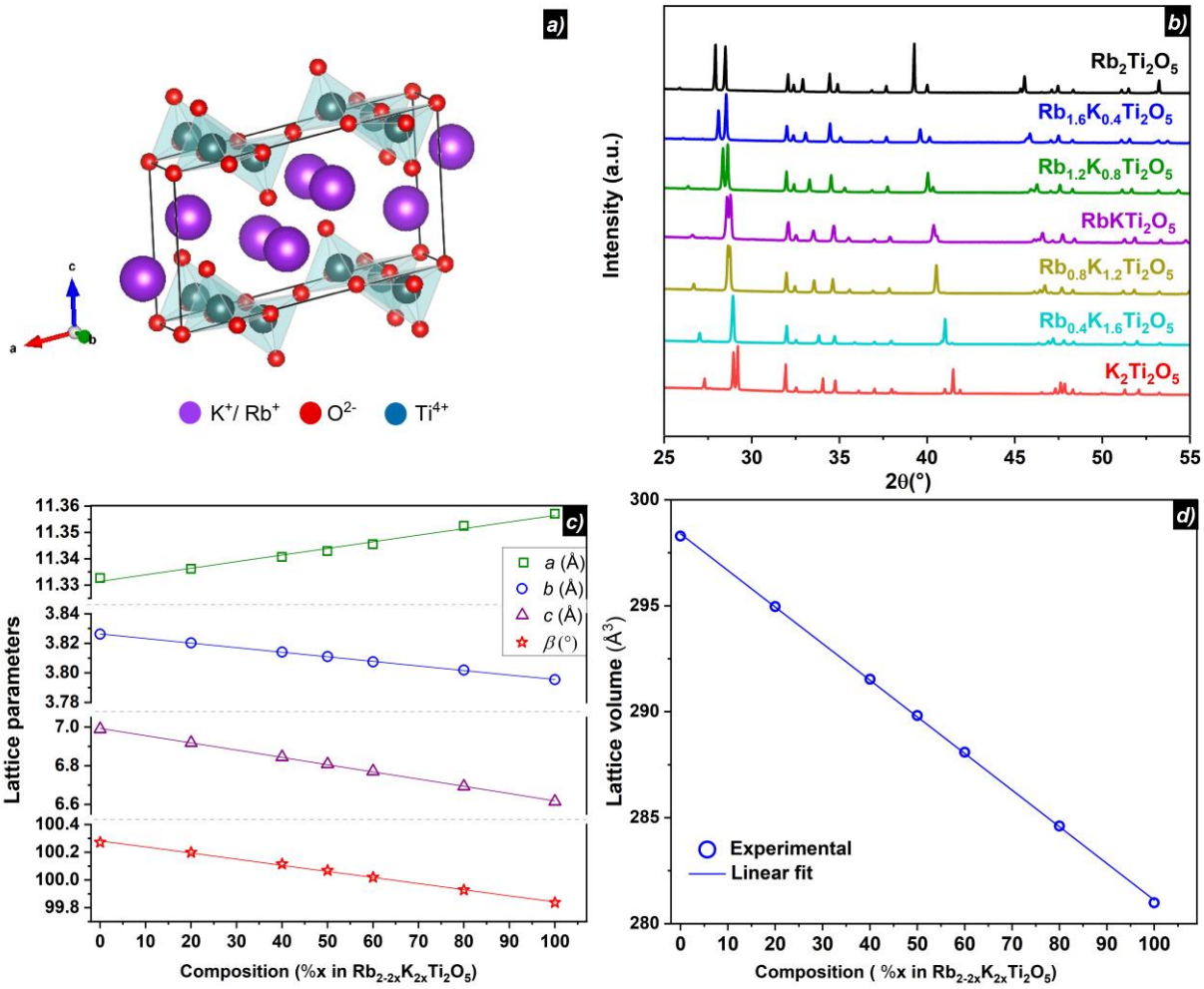

Figure 1: (a) Crystal structure of $M_2Ti_2O_5$ (figure S1 shows the crystal structure with different orientations, stressing out the titanium oxide double chains and the 2D staking). (b) XRD patterns of as-synthesized $Rb_{2-2x}K_{2x}Ti_2O_5$ samples (refinements are shown in supplementary information, fig. S2 to S8). (c) Lattice parameters in the series $Rb_{2-2x}K_{2x}Ti_2O_5$ as a function of the potassium content. (d) lattice cell volume in the series $Rb_{2-2x}K_{2x}Ti_2O_5$ as a function of the potassium content. Error bars in figures c and d are smaller than the size of the symbols

Figure 1b shows the XRD patterns of the as-synthesized $Rb_{2-2x}K_{2x}Ti_2O_5$ series. The Le Bail refinements shown in figures S2 to S8 indicate that all samples are single-phase (in the detection limit of XRD) and crystallize in the same monoclinic space group C2/m, which shows that a complete solid-solution exists between $Rb_2Ti_2O_5$ and $K_2Ti_2O_5$. A shift of some Bragg peaks towards larger angles is observed when the potassium fraction increases, while others remain constant or even shift to lower angles, indicating an anisotropic change in the lattice parameters. Indeed, the refinements show that the increase of potassium concentration within the series leads to a linear evolution of the lattice parameters and angle β, in good agreement with Vegard's law (Figure 1c). Collectively, this evolution leads to a contraction of the unit cell volume of 5.8% when the concentration of potassium increases, which is expected from the ionic radius of K^+ being significantly smaller than that of Rb^+, 138 pm as compared to 152 pm (Figure 1d). Interestingly, it can be seen in Figure 1c that the lattice parameter *c* is much

more sensitive to the respective concentration of alkali elements than *a* and *b*, with a decrease of 5.4% when going from $Rb_2Ti_2O_5$ to $K_2Ti_2O_5$ as compared to 0.8% for *b*, while a surprisingly increase by 0.2% is observed for *a*. This stronger dependence of *c* on the composition could most probably be explained by the crystal structure. Indeed, as it can be observed in Figure 1a (and figures S1), the crystal structure of $M_2Ti_2O_5$ consists of a stacking of titanium oxide and alkali ions layers along the *c*-axis of the unit cell. As mentioned, a counterintuitive increase of *a* is observed when increasing the potassium fraction, which is consistent with the values reported in the literature for the parent compounds $Rb_2Ti_2O_5$ and $K_2Ti_2O_5$[2,3]. The data presented here do not allow for an unambiguous explanation of this observation, which remains out of the scope of our study. However, such behavior would undoubtedly merit further investigation, coupling theoretical calculations with in-depth structural and dynamic characterisation, as it might influence the physical properties of these materials.

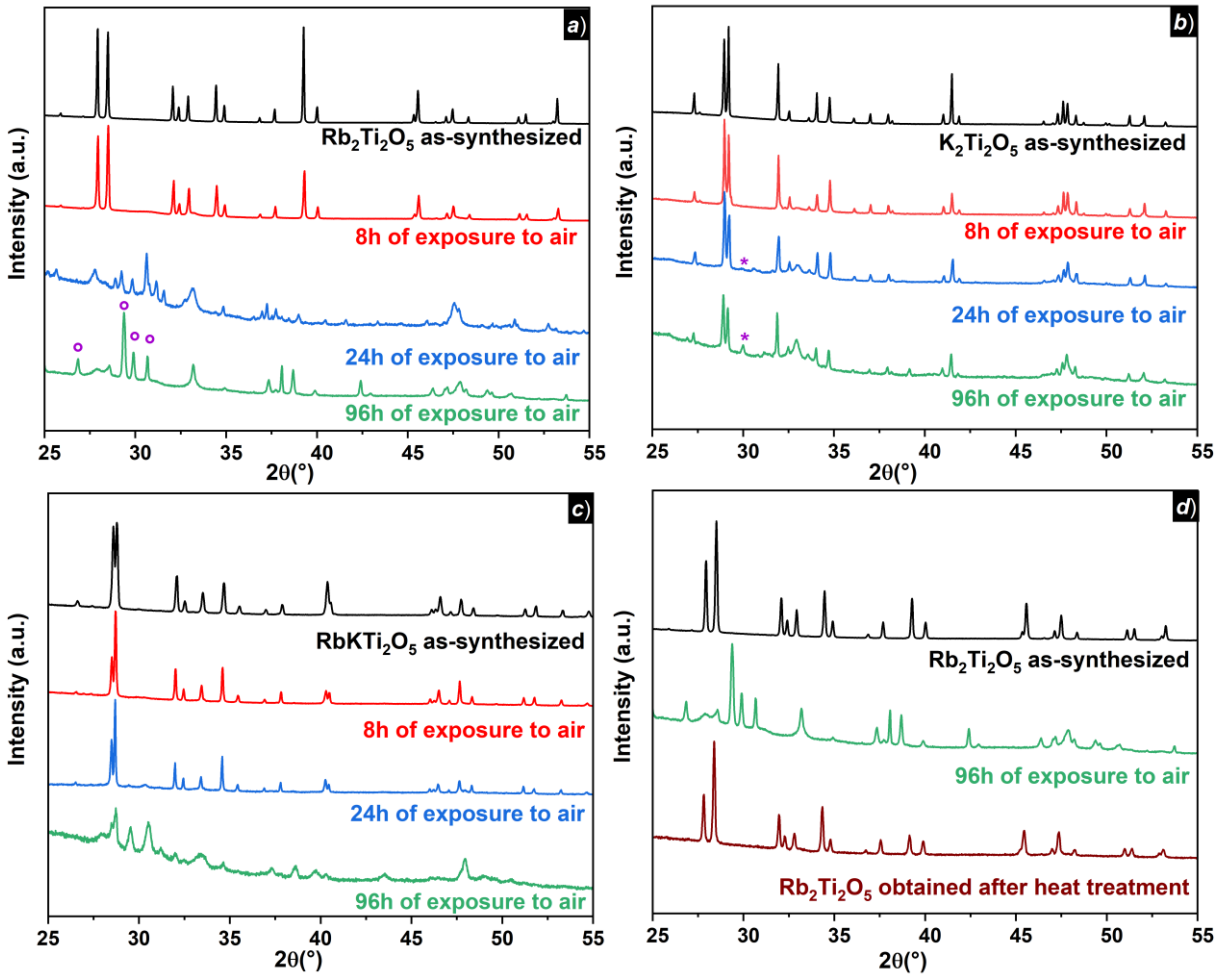

Figure 2: (a) XRD patterns of $Rb_2Ti_2O_5$, as-synthesized and after exposure to ambient air. (b) XRD patterns of $K_2Ti_2O_5$, as-synthesized and after exposure to ambient air. (c) XRD patterns of $RbKTi_2O_5$, as-synthesized and after exposure to ambient air. (d) XRD patterns of as-synthesized $Rb_2Ti_2O_5$, a sample exposed to ambient air during 96h, and of a sample exposed to ambient air during 14 days followed by a heat treatment of 1h at 800°C. Importantly, although the progressive substitution of the two alkalis (potassium and rubidium) affects the relative intensity of the diffraction peaks of the different isostructural phases, this systematic variation is shielded by the random contribution due to the

preferential orientation of the crystallites. In particular, the significant changes of the relative intensities of the (2 0 2) and (1 1 1) peaks located around 2θ=28-29° observed from one sample to another are mostly due to differences of preferential orientation of the crystallites originating from the anisotropic shape of the particles and the Bragg-Brentano geometry used for the XRD analysis. Indeed, *for these two specific peaks*, the relative intensity difference depends only slightly (a few percent) on the nature of the alkali element. Therefore, the observed variations should be considered as artefacts. In figures a and b, (°) and (*) symbols correspond to the main peaks of $RbHCO_3$ and $KHCO_3$ bicarbonates respectively.

In a previous study, De Sousa *et al.*[13] observed from XRD characterizations that two different $Rb_2Ti_2O_5$ samples, one dehydrated consisting of a collection of small single crystals and one exposed to ambient air for 9 hours, did not exhibit any difference in terms of lattice parameters. However, they noted the emergence of some broad peaks around 2θ=30° and a significant weight gain in TGA, which they attributed to hydration. To confirm this observation and study the influence of the alkali element's nature, we conducted several exposures to ambient air of $Rb_{2-2x}K_{2x}Ti_2O_5$ (x = 0, 1 and 2) powder samples by varying exposure times, namely during 0h, 8h, 24h, and 96h (Figure 2). Comparing Figure 2a and 2b, a significant difference between the behaviors of $Rb_2Ti_2O_5$ and $K_2Ti_2O_5$ can be noticed. In the case of $Rb_2Ti_2O_5$, no significant evolution is observed after 8h of exposure to ambient air, which is consistent with the previous observations made by De Sousa *et al*[13]. However, after 24 hours, the Bragg peaks associated with the crystalline phase $Rb_2Ti_2O_5$ totally disappear, replaced by other peaks (some of them being very broad), indicating the degradation of this compound into other phases. Then, the nature of the phases that are present keeps on changing after 96h of exposure. A similar phenomenon is observed for $K_2Ti_2O_5$, but with a much slower kinetic. Indeed, some new peaks start appearing after 24 hours of exposure, although their intensity is low. Moreover, the Bragg peaks associated with the crystalline phase of $K_2Ti_2O_5$ persist even after 96 hours of exposure to ambient air and are still well defined, although some of them start broadening with a decrease of intensity.
XRD observations show that $Rb_2Ti_2O_5$ does not degrade into one single phase, but into several ones successively, corresponding to reactions with both H_2O and CO_2. The diffraction pattern of the powder exposed for 24 hours shows that the $Rb_2Ti_2O_5$ crystalline phase is almost absent and that one or more secondary phases appear, in addition to peaks broadening. As illustrated in Figure 2a, after 24 hours of exposure, several phases are formed, including $RbHCO_3$, initially with Bragg peaks of low intensity but becoming predominant after 96 hours of exposure to ambient air (the main peaks of $RbHCO_3$ are indicated by (°) in Figure 2a). This indicates that the compound first decomposes into multiple phases, including an intermediate carbonate phase that appears to be less stable than $RbHCO_3$. Then, the compound transforms entirely into $RbHCO_3$ as well as an unidentified secondary phase with broad peaks and limited intensity (see Figure 2a and S9). Regarding $K_2Ti_2O_5$, alongside the significantly slower degradation kinetics as compared to $Rb_2Ti_2O_5$, the XRD patterns reveal the presence of new peaks in addition to those of the crystalline $K_2Ti_2O_5$ phase. These peaks remain weaker than those of the main $K_2Ti_2O_5$ phase event after 96h. XRD analyses confirm that the second phase formed in $K_2Ti_2O_5$ exposed to ambient air is $KHCO_3$ (indicating by * in Figure 2b), which is thus similar to the situation occurring in $Rb_2Ti_2O_5$ for similar duration with the only difference being the alkali element involved (see Figure 2b, S10 and S11). Although these XRD analyses shown that the degradation of $Rb_2Ti_2O_5$ and $K_2Ti_2O_5$ unambiguously leads to the formation of alkali bicarbonates, they do not unable to draw any reliable conclusion about what happens to titanium, which may bee present either in an amorphous phase or in the new phase that is observed in the XRD patterns after 96h of exposure but has not been identified

due to the limited number of broad peaks (and which does not correspond to either rutile or anatase phases).

As for the mixed compound $RbKTi_2O_5$ (see Figure 2c), the decomposition kinetics surprisingly appears to be first slower than that of both parent compounds $Rb_2Ti_2O_5$ and $K_2Ti_2O_5$, for air exposure of 8 hours and 24 hours. Indeed, after 24-hour exposure, a limited broadening of the peaks is present, mainly in the range between 30 and 35°, but this broadening is much less pronounced than in the case of $Rb_2Ti_2O_5$ and $K_2Ti_2O_5$. However, although slower, the degradation mechanism appears similar to that of the other two compounds, involving the weakening of the intensity of the Bragg peaks of the $Rb_{2-2x}K_{2x}Ti_2O_5$ phase, and the appearance of secondary phases observed with the emergence of low-intensity peaks around $2\theta = 30°$. For longer durations, exposing the compound to ambient air for 96 hours leads to a severe acceleration of the degradation process. As it can be seen in Figure 2c, the $RbKTi_2O_5$ crystalline phase totally disappears after 96h, and the sample mostly consists of a mixture of the phases resulting from the degradation of $Rb_2Ti_2O_5$ and $K_2Ti_2O_5$.
Figure 2d shows an XRD pattern of $Rb_2Ti_2O_5$ exposed to air during 96h, and another pattern of the same sample after a heat treatment of one hour at 800°C. It is noteworthy that this thermal treatment (which is similar to the one used for the thermogravimetric analysis, see later) is sufficient to regenerate the crystalline phase $M_2Ti_2O_5$ with the same lattice parameters as the as-synthesized samples and without any secondary phase, a phenomenon consistently observed for all $Rb_{2-2x}K_{2x}Ti_2O_5$ compounds exposed to air. This shows that the degradation is reversible, which implies that no loss of titanium or alkali elements occurs during this process. This observation is consistent with previous observations made in the literature with $K_2Ti_2O_5$, where $K_2Ti_2O_5$ sample exposed to ambient atmosphere for several days could be regenerated after a thermal treatment at 700°C. In that former study, the hydration of powdered $K_2Ti_2O_5$ was achieved in water vapor saturated atmosphere at room temperature for a long exposure time, resulting in the total decomposition of the crystalline phase before the regeneration process at 700°C[15].

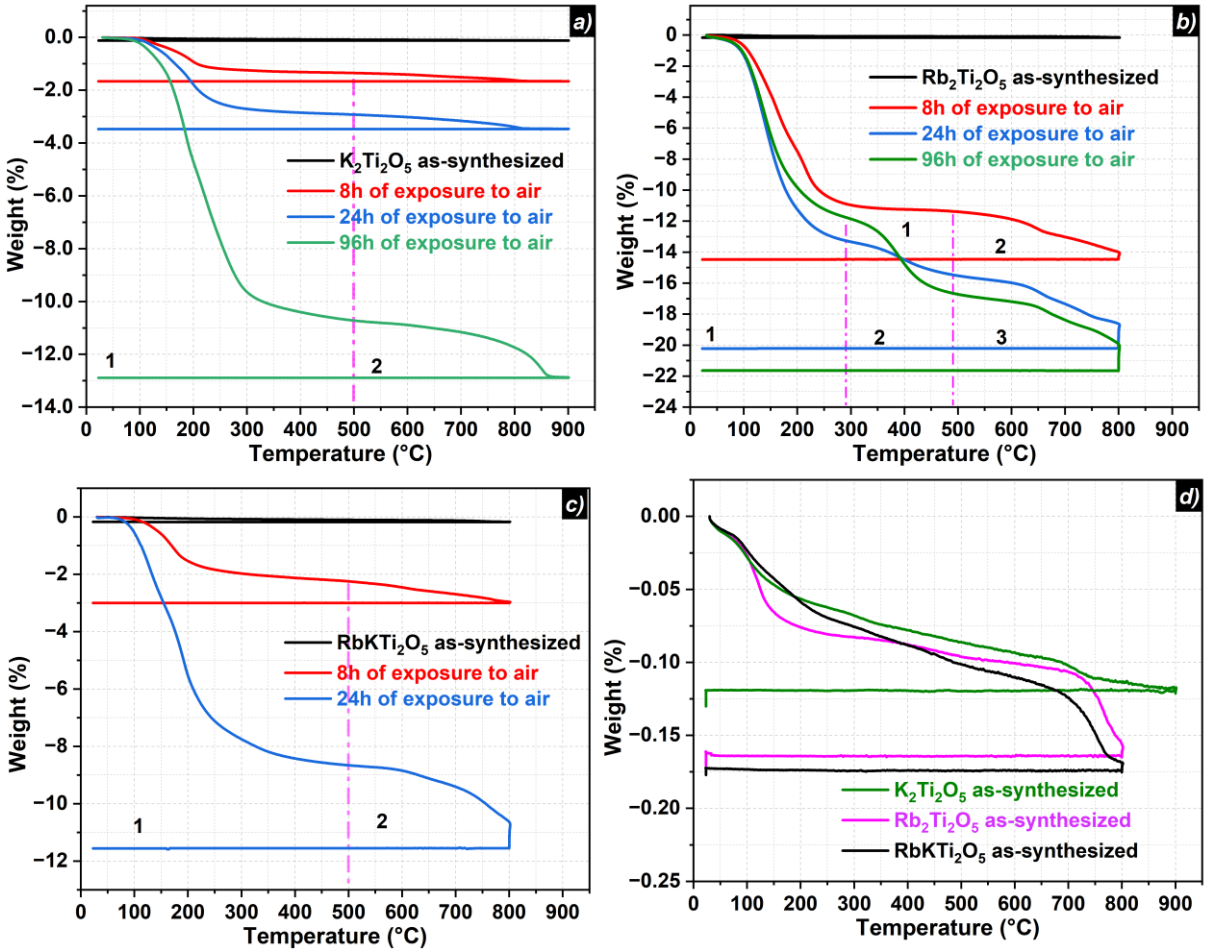

Figure 3: (a) Thermogravimetric analysis of $K_2Ti_2O_5$, as-synthesized and exposed to ambient air from 8h to 96h. (b) Thermogravimetric analysis of $Rb_2Ti_2O_5$, as-synthesized and exposed to ambient air from 8h to 96h. (c) Thermogravimetric analysis of $RbKTi_2O_5$, as-synthesized and exposed to ambient air from 8h to 24h. (d) Thermogravimetric analysis of as-synthesized $Rb_{2-2x}K_{2x}Ti_2O_5$ (x = 0, 0.5 and 1).

The results of thermogravimetric analysis, carried out using the same samples exposed to air as those used for X-ray diffraction measurements, are shown in Figure 3. As the XRD analysis performed after the heat treatment of 1h at 800°C has shown that the initial structure of the samples is fully restored (see Figure 2d), the weight losses observed during the TG analyses correspond exactly to the weight gain of the samples when exposed to ambient air. For all compositions, the observed weight losses increase monotonically as the samples are exposed to air for longer, with in each case at least two distinct steps. For all durations, $Rb_2Ti_2O_5$ exhibits a much larger loss than the other compounds, which is consistent with the quicker decomposition kinetic observed for this compound by XRD. For example, in the case of a 24-hour exposure to ambient air, the total weight loss for $Rb_2Ti_2O_5$ is 20.17%, compared with 3.47% and 11.55% for $K_2Ti_2O_5$ and $RbKTi_2O_5$, respectively. In addition, at a first glance the number of loss steps seems to vary from one curve to another, depending on the compound and the duration of exposure to air. It is noteworthy that in the case of $Rb_2Ti_2O_5$ exposed to air, the weight loss that occurs during the plateau at 800°C does not originate from alkali volatilization, as (i) it is negligible for the as-synthesized sample, (ii) the magnitude of this loss is a direct function of the duration of exposure, and (iii) this weight loss saturates before the end of the plateau (see Figure S12).

As shown in Figure 3d, as-synthesized $K_2Ti_2O_5$ exhibits a first continuous weight loss between 80°C and 650°C, followed by a second step between 650°C and 800°C, with a total loss of 0.12%. The same is observed for $Rb_2Ti_2O_5$ and $RbKTi_2O_5$, with 0.16% and 0.17% of total weight loss respectively. These weight losses for as-synthesized samples are very small, but they constitute an obvious signature of the extreme sensitivity of the compounds to H_2O and CO_2, as the handling time outside of the glovebox for these samples, which corresponds to the transfer from the furnace to the glovebox and then from the glovebox to the thermogravimetric analyzer, was of the order of one minute.

For $K_2Ti_2O_5$ powders exposed to air for 8 hours, 24 hours and 96 hours, two significant weight losses are observed, with values detailed in table 2. The first is centered between circa 100 and 300 °C (the values indicated in Table 2 are calculated between 80°C and 500°C), and the second between circa 750 and 850 °C (values in Table 2 calculated between 500°C and 900°C), see figure 3a.

Similarly, for the $Rb_2Ti_2O_5$ compound exposed to air for 8 hours, two distinct steps are observed within the same temperature range as $K_2Ti_2O_5$. Regarding samples exposed to air for 24 and 96 hours, at least three distinct steps are observed (Figure 3b). The first occurs between 80°C and approximately 300°C, the second between 300°C and 500°C, and the last between 600°C and 800°C. The values for each of them are detailed in Table 2. It is noteworthy that for every duration of exposure to ambient air, these values are significantly larger for $Rb_2Ti_2O_5$ than for $K_2Ti_2O_5$.

Last, the behavior of the mixed compound $RbKTi_2O_5$ is shown in Figure 3c. After exposure for 8 hours and 24 hours, this compound exhibits a slightly different behavior from the one observed for $K_2Ti_2O_5$, with additional losses similar to those observed for $Rb_2Ti_2O_5$ although less pronounced. The magnitude of the weight losses for every duration of exposure is also larger than the one observed for $K_2Ti_2O_5$, and lower than the one observed for $Rb_2Ti_2O_5$ (Table 2). Therefore, the behavior of this compound appears to be intermediate between those of $K_2Ti_2O_5$ and $Rb_2Ti_2O_5$.

$K_2Ti_2O_5$	1st loss (80°C - 500°C)	2nd loss (500°C - 900°C)	Total weight loss
as-synthesized	0.10%	0.02%	0.12%
8h of exposure to air	1.35%	0.31%	1.66%
24h of exposure to air	2.89%	0.58%	3.47%
96h of exposure to air	10.70%	2.20%	12.9%

$Rb_2Ti_2O_5$	1st loss	2^{nd} loss	3rd loss	Total weight loss
as-synthesized	0.12%	0.05%	/	0.17%

8h of exposure to air	11.39% (80°C – 500°C)	3.08% (500°C – 800°C)	/	14.47%
24h of exposure to air	13.60% (500°C – 300°C)	2.17% (300°C – 500°C)	4.40% (600°C – 800°C)	20.17%
96h of exposure to air	11.90% (500°C – 300°C)	5.47% (300°C – 500°C)	4.25% (600°C – 800°C)	21.62%

$RbKTi_2O_5$	1st loss (80°C – 500°C)	2^{nd} loss (500°C – 800°C)	Total weight loss
as-synthesized	0.11%	0.05%	0.17%
8h of exposure to air	2.24%	0.76%	3.00%
24h of exposure to air	8.56%	2.99%	11.55%

Table 2: Weight losses of $M_2Ti_2O_5$ after exposure to ambient air, obtained from TGA (Figure 3a, 3b and 3c).

The first step observed for all compositions can be attributed to their dehydration, occurring within the temperature range of 80 to 300°C. XRD analysis has evidenced the formation of bicarbonates for the compounds exposed to ambient air, as well as the regeneration of their crystalline structure after TGA at high temperature (800°C). This suggests that the weight loss at high temperature may be attributed to CO_2 departure. This conclusion is consistent with the decarbonation temperature for certain carbonate compounds such as K_2CO_3[17–19].

For both $Rb_2Ti_2O_5$ and $K_2Ti_2O_5$, the shape of the TGA curves and the different number of steps are consistent with the XRD observations described above. In the case of $Rb_2Ti_2O_5$ several successive steps are observed, consistent with the presence of several different rubidium/titanium hydro-carbonates, whereas in the case of $K_2Ti_2O_5$, the presence of $KHCO_3$ only is consistent with the observation of one single step in the TGA curve above 300°C. For the later compound, the two steps would thus correspond to the loss of water below 300°C and CO_2 at higher temperature.

The scenario suggested so far is confirmed by the infrared measurements as presented and discussed in the following section.

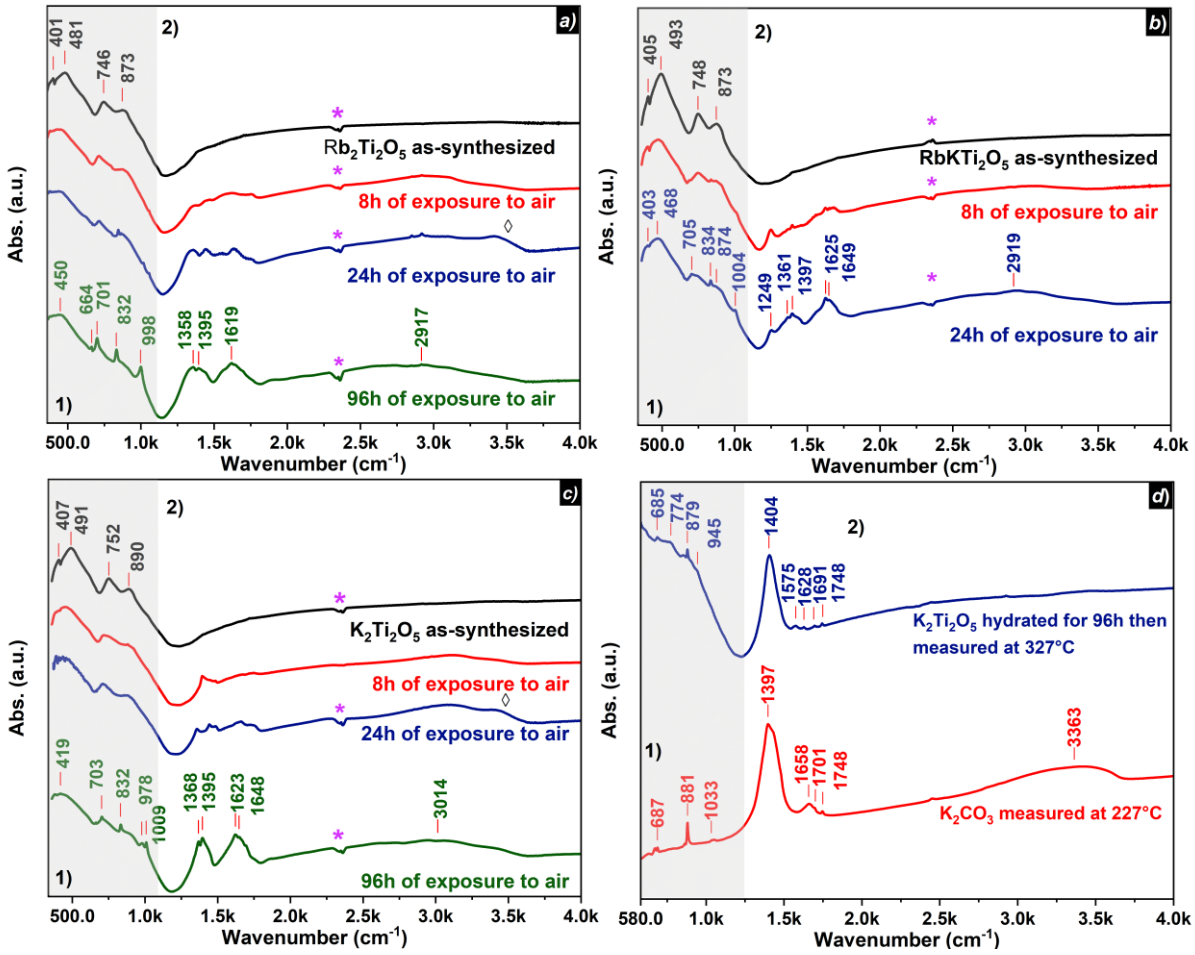

Figure 4: Room temperature IR spectra of $M_2Ti_2O_5$, as synthesized and after different times of exposure to ambient air. (a) $Rb_2Ti_2O_5$, (b) $RbKTi_2O_5$ and (c) $K_2Ti_2O_5$. (d) IR spectrum of $K_2Ti_2O_5$ after 96h of exposure to ambient air measured at 327°C, compared to IR spectrum of K_2CO_3 measured at 227°C. The small features indicated by (*) in figures a, b and c correspond to an imperfect compensation of the ambient CO_2 stretching vibration between the sample and the KBr reference pellets during the room-temperature measurements.

In Figure 4a, 4b and 4c, we report the IR spectra of $Rb_2Ti_2O_5$, $RbKTi_2O_5$ and $K_2Ti_2O_5$, for as-synthesized samples and for different durations of exposure to ambient air. The small positive and negative structures labeled with a star are due to the imperfect compensation of the ambient CO_2 stretching vibration between the sample and the KBr reference pellets. Two main spectral ranges can be distinguished: one at low wavenumbers (light gray shadow region labeled 1) between 360 and 1000 cm^{-1} and one at larger wavenumbers (labeled 2) between 1000 and 4000 cm^{-1}. The first one is characterized by the phonon signatures associated with the atomic collective dynamics of the crystalline Rb_2Ti_2O and $K_2Ti_2O_5$ lattices. Here, four main peaks can be seen in the as-synthesized samples (and in the samples exposed to ambient air for a limited time). The second one is characterized by the spectral signatures of OH^- and CO_3^{2-} functional groups vibrations. Notwithstanding some minor differences, all three compounds exhibit similar spectra and similar evolutions with respect to the exposure to ambient air. In region 1, the phononic features mostly originate from the vibrations of the TiO_5 pyramids and are thus only slightly affected by the nature of the alkali atoms present in the crystal structure. In this region, the exposure to ambient air results in the emergence of new sharp peaks that

were not present in the as-synthesized samples, and whose energies are very similar for all compounds (see for example the peak at ~832 cm^{-1} in the green curves of Figure 4a and 4c due to the insurgence of the carbonate and bicarbonate phases as can be appreciated in figure 5 and S21). This suggests that all three compounds undergo alterations of same natures. A similar behavior is observed in region 2 where several structured bands appear as a consequence of the air exposure. These bands become more and more intense as the exposure time increases. They can unambiguously be assigned to the carbonate and water bending and stretching vibrations, which are highly sensitive to the atomic environment[20–22]. Therefore, the differences between their respective energies and shapes from one compound to another might be attributed to the different alkali elements present in the three compounds. In the energy region between 1000 and 1800 cm^{-1}, the bending excitations of the water molecule at around 1600 cm^{-1} and the carbonate vibrations at around 1400 cm^{-1} become significant after exposure. A similar behavior is observed, at higher energy, for the large band at around 3000 cm^{-1} that originates from the water stretching vibrations[20,21].For $Rb_2Ti_2O_5$ and $K_2Ti_2O_5$, and to a much smaller extent for $RbKTi_2O_5$, a new broadband (indicated by an "◊" in Figures 4a and 4c) emerges after 24h of exposure. The position of this band corresponds to the energy of the stretching OH vibrations into the carbonate environment (see Figure 4d, red curve). This suggests that once the bicarbonates are formed, part of the ambient water molecules react with them. This band progressively disappears as the exposure time to air is extended. The infrared measurements confirm that the bicarbonates form as a consequence to the exposure to ambient air, and are not present in the as-synthesized compounds as residuals of the precursors. In a previous study, De Sousa *et al*[13] showed by thermogravimetric analysis that dehydrated crystalline $Rb_2Ti_2O_5$ does not react with CO_2 at room temperature. This suggests, in agreement with the present observations, that the compound requires the presence of water to react with CO_2. We can therefore conclude that, when exposed to ambient air, the crystalline compound simultaneously absorbs water and CO_2, thus starting the chemical reactions to form bicarbonates as confirmed by the XRD observations, as well as Ti-based unidentified crystalline or amorphous phase(s). This mechanism would be consistent with the strong sensitivity of $K_2Ti_2O_5$ to mild acid environments reported by Bamberger *et al*[15]. The IR spectra obtained for $Rb_2Ti_2O_5$ and $K_2Ti_2O_5$ exposed to ambient air for 96 hours (Figure 4a and 4c.) show great similarity with those of $KHCO_3$ and $RbHCO_3$ reported in the literature. All the vibrational modes indexed in the green curves of Figure 4a and 4c can be associated with CO_3^{2-}, OH^-, or CO_3^{2-} coupled to OH^- groups present in $KHCO_3$ and $RbHCO_3$[20,21,23] thus confirming the formation of bicarbonates in our samples. Regarding $K_2Ti_2O_5$, as mentioned above, the XRD measurements show the presence of $KHCO_3$ at room temperature after air exposure. As it will be seen in more details below, between T=110°C and T=377°C, infrared measurements show the progressive disappearance of structures associated with the bicarbonate $KHCO_3$ and the gradual emergence of peaks associated with the carbonate K_2CO_3. The $KHCO_3$ infrared signature disappears completely at T=377°C. For temperatures higher than 300°C, the thermogravimetric analysis reveals a single step loss of mass at high-temperature linked to decarbonation. This whole scenario suggests that $KHCO_3$ and K_2CO_3 are the only carbonates formed during $K_2Ti_2O_5$ degradation. However, in the case of $Rb_2Ti_2O_5$ exposed to air for 24 hours, the situation is more complicated. As shown in Figure 3b, several successive stages of mass loss are observed in the TGA curves, and at least two different phases are detected by XRD (Figure 2a). In addition, the IR vibrational bands are broader than those of $K_2Ti_2O_5$ (see Figure 4a and 4c), suggesting the possible formation of more different hydrogeno-carbonates when the compound is exposed to ambient air. However, after an intermediate behavior, $RbHCO_3$ emerges as the predominant phase after 96h hours of exposure to ambient air (Figure S9 and 4a).

Regarding the mixed compound $RbKTi_2O_5$ (Figure 4b), IR spectra show an intermediate behavior between $Rb_2Ti_2O_5$ and $K_2Ti_2O_5$. After 8 hours exposure to ambient air, water absorption can be detected from the broad band around 2900 cm^{-1}. Bicarbonate peaks also appear and become more intense after 24 hours of exposure (see for example the structures at 705 cm^{-1}, 834 cm^{-1} and 1397 cm^{-1}). Differently to what is observed in $Rb_2Ti_2O_5$ and $K_2Ti_2O_5$, starting from 8h of exposure, a peak at 1249 cm^{-1} is detected in $RbKTi_2O_5$. Although not visible in Figure 4c, this peak is present in $K_2Ti_2O_5$ exposed to air in the case of a measurement carried out on $K_2Ti_2O_5$ + KBr pellet left in air several days (see Figure S13). We can then argue that the degradation kinetics may play a role in the detection of this small absorption that could be screened by the 1370 cm^{-1} band whose intensity and width increase fast in a rapid kinetics.

As shown above, we observed differences in the vibrational modes of alkali carbonate K_2CO_3 and Rb_2CO_3 and those of the $M_2Ti_2O_5$ compounds exposed to air at room temperature. To investigate this further, we studied the effect of temperature on the IR spectrum of $K_2Ti_2O_5$ as compared to K_2CO_3. $K_2Ti_2O_5$ was measured at 327°C (above the first weight loss observed by TGA) and K_2CO_3 at 227°C, as shown in Figure 4d. At this temperature, the spectrum of $K_2Ti_2O_5$ exposed to air becomes similar to that of K_2CO_3. Indeed, the characteristic carbonate peaks at around 1400 cm^{-1}, 880 cm^{-1} and 680 cm^{-1} appear clearly in both samples.

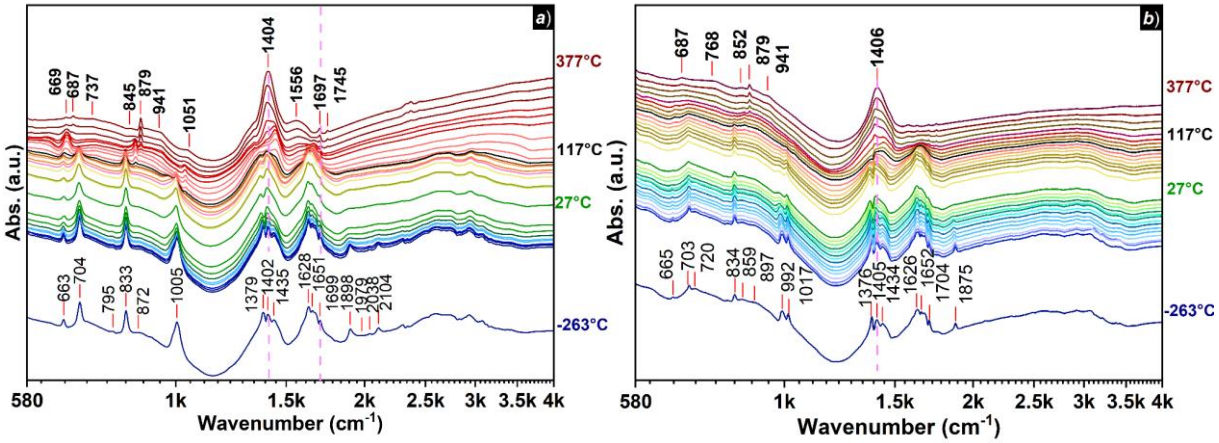

Figure 5: in-situ IR spectra from -263°C to 377°C of (a) $Rb_2Ti_2O_5$ and (b) $K_2Ti_2O_5$ previously exposed to ambient air during 96h. The samples were first cooled down to -263°C and then measured while heating up to 377°C. (note that for better clarity, the x-axis scale is logarithmic and the first value is explicitly shown, differing from the scale used in Figure 4)

In order to understand the chemical evolution of strongly hydrated $Rb_2Ti_2O_5$ and $K_2Ti_2O_5$ samples (96h of exposition), we performed a series of temperature-dependent IR measurements between -263 °C and 377 °C. The results are reported in Figure 5a for $Rb_2Ti_2O_5$ and Figure 5b for $K_2Ti_2O_5$. We started each thermal cycle with cooling down to the lowest attainable temperature and then heating up to the highest temperature with measurements every 10 degrees. At low temperature, no relevant modifications of the spectra are observed while at high temperature the spectroscopic profile evolves significantly as compared to room temperature.

For both compounds, we observe a clear decrease of the intensity of the vibrational modes associated with the OH stretching (~ 3000 cm^{-1}) and bending (~ 1600 cm^{-1}) upon heating, as well as of the peaks

located around 1375 cm^{-1}, 1435 cm^{-1}. In this region, we also observe the growth of a characteristic carbonate peak, centered at 1404 cm^{-1} for $Rb_2Ti_2O_5$ and 1406 cm^{-1} for $K_2Ti_2O_5$. At low frequencies, characteristic $RbHCO_3$ peaks at 663 cm^{-1}, 704 cm^{-1}, 833 cm^{-1} and 1005 cm^{-1} (see Figure 5a) and characteristic $KHCO_3$ peaks at 665 cm^{-1}, 703 cm^{-1}, 834 cm^{-1}, 992 cm^{-1} and 1017 cm^{-1} (Figure 5b) are present at low temperature. These peaks are no longer present at 377°C where they are replaced by other sharp bands characteristic of K_2CO_3 and Rb_2CO_3, namely 687 cm^{-1}, 879 cm^{-1}, 941 cm^{-1} and 1051 cm^{-1} for Rb_2CO_3, and 687 cm^{-1}, 852 cm^{-1}, 879 cm^{-1} and 941 cm^{-1} for K_2CO_3 (see Figure S14). From these observations, we can confirm i) the presence of bicarbonate in compounds exposed to ambient air, and ii) the presence of carbonate and the absence of water in the compound for temperatures higher than 227°C. This finding is consistent with what reported in literature, i.e. starting from 200°C $KHCO_3$ decomposes into K_2CO_3, H_2O and CO_2[17,24]. We can so argue for $KHCO_3$ (and by analogy for $RbHCO_3$) a chemical evolution as described by the following reactions starting from T= 117°C:

$$2\ KHCO_3 = K_2CO_3 + H_2O + CO_2$$
$$2\ RbHCO_3 = Rb_2CO_3 + H_2O + CO_2$$

These findings, together with those obtained from thermogravimetric analysis (see Figure 3) and X-ray diffraction (see Figure 2), allow to clarify the high temperature evolution of hydrated $K_2Ti_2O_5$. Specifically, between 100°C and 500°C, the first mass drop is due to the carbonates formation with consequently loss of H_2O + CO_2. While, at high temperature, the second mass drop is due to the CO_2 loss, released during the "reformation" of the crystalline compound $K_2Ti_2O_5$. Regarding $Rb_2Ti_2O_5$, the scenario is more complex given the presence of several phases in XRD and several steps losses in TGA. Here we can only assert that starting from T=120°C the compound loses water and CO_2, and that the last loss is probably linked to CO_2 released when the crystalline $Rb_2Ti_2O_5$ is reformed. However, no further conclusion can be proposed at this stage about the intermediate reactions.

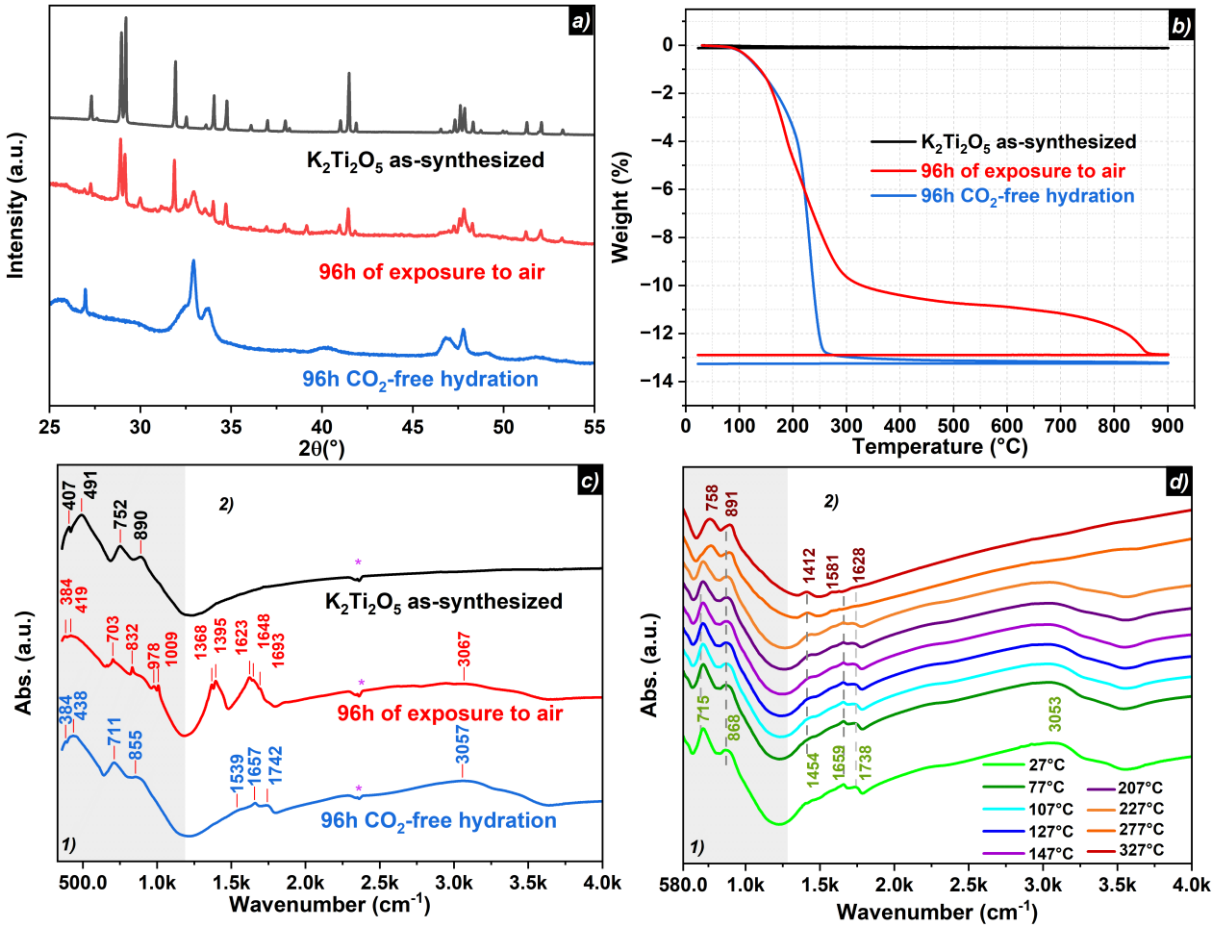

Figure 6: (a) XRD patterns of as-synthesized $K_2Ti_2O_5$, compared to the XRD patterns after 96h of exposure to ambient air and 96h of CO_2-free hydration. (b) Weight loss measured by TGA for as-synthesized $K_2Ti_2O_5$, after 96h of exposure to ambient air, and after 96h of CO_2-free hydration. (c) Influence of the hydration condition (ambient air or CO_2-free) on the IR spectrum of $K_2Ti_2O_5$. (d) in-situ IR spectra from 27°C to 327°C of $K_2Ti_2O_5$ after 96h of CO_2-free hydration.

As we have seen, both X-ray diffraction and infrared spectroscopy measurements evidence the presence of bicarbonates and water, for the compounds exposed to ambient air. In order to better understand the mechanisms of degradation, the same experiments have been carried out on samples hydrated under CO_2-free conditions (Figure 6). Specifically, hydration experiments were performed in a closed system under an argon atmosphere, as described in the experimental section. Although no evolution of the lattice parameters was observed, a broadening of the Bragg peaks can be seen in the diffraction patterns of the samples hydrated without CO_2 as compared to the as-synthesized ones, suggesting that hydration induced structural changes (Figure 6a and S15). Notably, after 96 hours of hydration, no bicarbonate phase was detected in any of the compounds, although residual crystalline phase peaks were observed for $Rb_2Ti_2O_5$ and $RbKTi_2O_5$ (Figure 6a and S15). These results confirm that the amount of residual carbonates coming from the precursors were negligible in the as-synthesized

samples, and that the bicarbonates observed in the XRD patterns and IR spectra of the samples exposed to ambient air do originate from the reaction of the compounds with CO_2 from the atmosphere, as concluded above.

Figure 6b and S16 show comparisons of the weight losses of $Rb_{2-2x}K_{2x}Ti_2O_5$ samples exposed to ambient air or hydrated in a CO_2-free environment. As expected, the second mass loss that occurs around 700°C in Figure 3 is not present in the absence of CO_2 (Figure 6b and S16). For instance, when $K_2Ti_2O_5$ is hydrated for 24h in a CO_2-free environment, only an initial significant mass loss of approximately 10.44% is observed. In contrast, for the same duration, $K_2Ti_2O_5$ exposed to ambient air presents two distinct mass losses (see Figure 3a). This observation unambiguously confirms that the second loss of $K_2Ti_2O_5$ exposed to ambient air is linked to CO_2. Similar trends are observed for $Rb_2Ti_2O_5$ and $RbKTi_2O_5$. Note that it is not possible to make a direct comparison of the total weight loss of samples exposed to ambient air or hydrated in a CO_2 free environment and only the trends can be compared. This is because the humidity rate during the sample exposure is different (see experimental methods). Looking at the influence of the nature of the alkali element, it appears that the hygroscopicity of $Rb_2Ti_2O_5$ is significantly higher than that of the other compounds, as shown in Figure S16, where a respective incorporation of 1.47, 2.69 and 1.22 moles of water molecules per 1 mole of $K_2Ti_2O_5$, $Rb_2Ti_2O_5$ and $RbKTi_2O_5$ is observed after 24 hours. For all samples, the modification of the crystalline phase starts after about 8 hours of CO_2-free hydration, with the appearance of unidentified diffraction peaks (Figure 6a and S15). However, the kinetics of the crystalline structure degradation appear to be slightly slower for $Rb_2Ti_2O_5$ compounds hydrated without CO_2 compared to $K_2Ti_2O_5$, as the Bragg peaks associated with the $Rb_2Ti_2O_5$ crystalline phase are still detected after 96 hours of hydration, although their intensity is low (Figure S15a), which is not the case for $K_2Ti_2O_5$. For the latter, a decrease of the intensity of the peaks related to its crystalline phase is observed after 8 hours of hydration, as well as the emergence of an unidentified secondary phase (see Figure 6a). After this first stage, the crystalline structure of $K_2Ti_2O_5$ degrades more rapidly than that of $Rb_2Ti_2O_5$. This is the opposite to what is observed when exposed to ambient air. Finally, the behavior of the mixed compound $RbKTi_2O_5$ does not show particular changes when hydrated with or without CO_2. We can therefore conclude that, at first glance, $Rb_2Ti_2O_5$ degrades faster in the presence of CO_2 than $K_2Ti_2O_5$, while the latter is more sensitive to H_2O in the absence of CO_2.

Figure 6 compares the IR spectra obtained for as-synthesized $K_2Ti_2O_5$, for $K_2Ti_2O_5$ exposed to ambient air for 96 hours, and for $K_2Ti_2O_5$ hydrated in a CO_2-free atmosphere for the same duration. The three spectra differ significantly. The spectrum of as-synthesized $K_2Ti_2O_5$ exhibits only 4 bands in the range of 380-1000 cm^{-1} associated with the crystalline structure, whereas the characteristic carbonate bands around 1400 cm^{-1} are present for $K_2Ti_2O_5$ exposed to air, as detailed above. The IR spectrum of CO_2-

free hydrated $K_2Ti_2O_5$ exhibits the presence of bands associated with water, with stretching around 3000 cm^{-1} and bending at 1600 cm^{-1}, but no peaks characteristic of the carbonates previously identified around 1400 cm^{-1}. Moreover, phonon-associated peaks are still present, with a slight shift as compared to the as-synthesized sample despite the absence of the $K_2Ti_2O_5$ crystalline phase in the XRD pattern (Figure 6a), which seems to indicate that nanodomains with $K_2Ti_2O_5$ crystal structure are still present although undetectable using XRD. These observations once again confirm that $K_2Ti_2O_5$, when exposed to air, reacts with the CO_2 in the ambient atmosphere, as the bicarbonate vibration modes are not present in the IR spectrum without CO_2. Similar observations can be made regarding $Rb_2Ti_2O_5$ and $RbKTi_2O_5$ compounds (Figure S17). We observed that when $M_2Ti_2O_5$ samples are exposed to ambient air, bicarbonates are formed, while their hydration in a CO_2-free atmosphere leads to the formation of one or several phases that have not been identified yet. Possible candidate could have been alkali hydroxides. In figure S21, we compare the room temperature IR spectra of $M_2Ti_2O_5$, M_2CO_3, MOH, and $K_2Ti_2O_5$ hydrated without CO_2. As it can be seen here, the vibration modes of RbOH and KOH are very different from those observed in the hydrated $M_2Ti_2O_5$ compounds, which rules out a possible role of alkali hydroxides in the degradation mechanism.

In-situ temperature dependent IR measurements of a $K_2Ti_2O_5$ sample hydrated during 96h in a CO_2-free environment confirm these conclusions (see Figure 6d). At 27°C, two peaks associated with phonons were identified at 868 cm^{-1} and 715 cm^{-1}, as well as two bands at 1660 cm^{-1} and 1738 cm^{-1} and a broad band around 3050 cm^{-1} associated with molecular water. When increasing temperature, the intensity of these bands decreases, until they disappear completely around 227°C. Note that some very weak peaks, different from those of the water molecule, appear upon heating at 1412 cm^{-1}, 1581 cm^{-1} and 1626 cm^{-1}, corresponding to the vibration mode bonds of the carbonate K_2CO_3. They constitute a clear signature of the extreme sensitivity of the hydrated samples to atmospheric CO_2, as they should originate from the handling of samples in air that did not exceed a couple of minutes, corresponding to their transfer from the glovebox to the IR spectrometer, or from the presence of small residual amounts of CO_2 in the reaction vial. A similar experiment was performed using $Rb_2Ti_2O_5$ hydrated in a CO_2-free environment for 6h or 96h (Figure S18 and S19). For the samples hydrated for 96 hours, broad bands are observed in the range of 1200-1800 cm^{-1}, indicating the presence of water and bicarbonates, although the intensity of the bicarbonate peaks is low as compared to the compound exposed to air for 96 hours (Figure 5b), their presence indicates here again the extreme sensitivity of the hydrated compound to CO_2. Additionally, the phonon region between 580 cm^{-1} and 1000 cm^{-1} appears to be significantly affected by the hydration, with very weak intensity, consistent with XRD observations showing very weak peaks of the crystalline phase (see Figure S15a). However, in the case of the sample hydrated for 6 hours (Figure S18), the phonon peaks are clearly present, consistent with

XRD observations (Figure S20). Besides, after 227°C heating, no water can be detected, and the characteristic carbonate peak around 1400 cm^{-1} emerges with very low intensity (Figure S18), similar to $K_2Ti_2O_5$. Interestingly, our IR measurements of $K_2Ti_2O_5$ samples show characteristic peaks of the phonon structures for every exposure time. This result can be appreciated in Figure 6c-d and S19. Moreover, it is also possible to notice in figure 6d the sudden hardening of the modes à ~715 et ~870 cm^{-1} for temperatures higher than or equal to 277°C, that is, when the sample dehydrates. This suggests a change affecting the Ti-O collective vibrations of the TiO_5 pyramids related to the loss of water molecules. Importantly, the same sample has a structure that is clearly different from the crystal structure of as synthesized $K_2Ti_2O_5$, as can be seen by looking at Figure 6a. Considering these results, the only hypothesis we can suggest is that the compound hydrated in CO_2 free conditions undergoes a modification that does not completely compromise the long-range order. Although the coordination and local structure are different (pyramids as compared to octahedra), this observation is somehow reminiscent of those made by Kang et al. in ref 25. In this study, the authors show the combination of short-range and partial long-range order in a layered hydrate titanate, supporting the formation of a fibrous-type particle aggregate. The XRD pattern of their H-titanate exhibits broad features similar to those shown in Figure 6a for $K_2Ti_2O_5$ after 96h of hydration without CO_2. Although our observations do not enable us to unambiguously determine what kind of evolution titanium undergoes in $M_2Ti_2O_5$, we can state that the pyramidal organization of TiO_5 is always present, at least in nanoscale cluster form, as evidenced by the phonon structures observed in the IR spectrum.

Conclusion :

To conclude, we have investigated the degradation of $Rb_{2-2x}K_{2x}Ti_2O_5$ compounds exposed to ambient air, and their respective reactivity with H_2O and CO_2, coupling thermogravimetric analysis, X-ray diffraction and infrared spectroscopy. These observations showed that upon exposure to ambient air, the degradation of the crystal structure is linked to the formation of bicarbonate phases, namely $KHCO_3$ and $RbHCO_3$ in the case of $K_2Ti_2O_5$ and $Rb_2Ti_2O_5$ respectively. For $Rb_2Ti_2O_5$, differently from $K_2Ti_2O_5$, several intermediate phases are also observed that gradually evolve towards predominant $RbHCO_3$. Moreover, we observed a slower degradation kinetic for the potassium titanate as compared to the rubidium one. Interestingly, these bicarbonates do not form in the case of dry samples, as reported in literature[13]. This implies that, when exposed to ambient air, the samples first hydrate by reacting with water vapor and then react with the ambient CO_2. Surprisingly, in the absence of CO_2, the crystal structure of $K_2Ti_2O_5$ degrades faster than that of $Rb_2Ti_2O_5$, although the latter absorbs water more efficiently. Independently of the alkali element, the lattice parameters of the $M_2Ti_2O_5$ phase are not affected by hydration, despite the progressive emergence of other phases in the diffraction patterns

and the influence of hydration on the energy of phononic modes (Table S1). At a first glance, the fact that the lattice parameters do not change could indicate that the overall structure remains unchanged and that no water molecule is incorporated within the crystal structure. The observed $M_2Ti_2O_5$ phase in the diffraction patterns of samples exposed to ambient air of CO_2-free humid atmosphere would thus correspond to grains that have not been degraded yet. However, it would not be consistent with the ionic conductivity measurements reported in ref. 13. In that context, theoretical calculations could provide further insights into the bonding mechanisms of hydrated compounds, and some estimations of the possible influence on the lattice parameters of water molecules introduced within the unit cells. Nevertheless, the new information reported in this work and related to the degradation mechanisms of $Rb_{2-2x}K_{2x}Ti_2O_5$ compounds exposed to ambient air, as well as their reactivity with H_2O and CO_2, are of significant interest for design strategies and optimization of the properties of these materials for functional applications.

Supporting Information:

Supporting information include figure, and tables that complement and illustrate our analyses, organized in the order they appear in the text. Figure S1 present the crystalline structure in different spatial directions, providing a detailed view of the atomic organization. Figures S2 to S8 present the various Le Bail refinements performed on the solid solutions $Rb_{2-2x}K_{2x}Ti_2O_5$, which enabled us to determine the lattice parameters of these materials. Figures S9 to S11 display the diffraction patterns of $Rb_2Ti_2O_5$ and $K_2Ti_2O_5$ exposed to the air, confirming the presence of carbonates in the degraded compounds. Figures S12 to S22 include various thermogravimetric analyses (TGA), X-ray diffraction (XRD) patterns, and infrared (IR) spectra to illustrate the evolution of the compounds in a CO_2-free atmosphere. (PDF)

Acknowledgments:

The authors gratefully acknowledge the French Agence Nationale de la Recherche (ANR) for funding, through the project MIMETIX (ANR 21-CE50-0035-02). We also acknowledge Yusuf Tokdemir for his help with sample synthesis, and Keevin Beneut for his help in preparing the temperature IR set-up. We are grateful to Nita Dragoe and Benoit Baptiste for fruitful discussions, Ludovic Delbes for his assistance in conducting XRD measurements, and Eric Elkaim for his support with XRD measurement and for the insightful discussions.

References

(1) Andersson, S.; Wadsley, A. D. Five Co-Ordinated Titanium in $K_2Ti_2O_5$. *Nature* **1960**, *187* (4736), 499–500.
(2) Andersson, S.; Wadsley, A. D.; Nilsson, R.; Olsen, G. E.; Pedersen, C.; Toft, J. The Crystal Structure of $K_2Ti_2O_5$. *Acta Chem. Scand.* **1961**, *15*, 663–669.
(3) Federicci, R.; Baptiste, B.; Finocchi, F.; Popa, F.; Brohan, L.; Béneut, K.; Giura, P.; Rousse, G.; Descamps-Mandine, A.; Douillard, T.; Shukla, A.; Leridon, B. The Crystal Structure of $Rb_2Ti_2O_5$. *Acta Cryst B* **2017**, *73* (6), 1142–1150.
(4) Chen, G.; Si, R.; Li, T.; Chen, P.; Wei, K.; Xie, X.; Chen, C.; Wang, C. Superior Linear Response of $K_2Ti_2O_5$ in Low and Medium Humidity Ranges. *ACS Applied Electronic Materials* **2021**, *3* (8), 3445-3450.
(5) Wang, Q.; Chung, J. S. NOx Storage and Reduction over Cu/$K_2Ti_2O_5$ in a Wide Temperature Range: Activity, Characterization, and Mechanism. *Applied Catalysis A: General* **2009**, *358* (1), 59–64.
(6) Zhao, S.; Dong, L.; Sun, B.; Yan, K.; Zhang, J.; Wan, S.; He, F.; Munroe, P.; Notten, P. H. L.; Wang, G. $K_2Ti_2O_5$@C Microspheres with Enhanced K_+ Intercalation Pseudocapacitance Ensuring Fast Potassium Storage and Long-Term Cycling Stability. *Small* **2020**, *16* (4), 1906131.
(7) Lin, L.; Hu, J.; Liu, J.; He, X.; Li, B.; Li, X. Selective Ammonium Removal from Synthetic Wastewater by Flow-Electrode Capacitive Deionization Using a Novel $K_2Ti_2O_5$-Activated Carbon Mixture Electrode. *Environ. Sci. Technol.* **2020**, *54* (19), 12723–12731.
(8) Zheng, Q.; Huang, L.; Zhang, Y.; Wang, J.; Zhao, C.-Z.; Zhang, Q.; Zheng, W.; Cao, D.; O'Hare, D.; Wang, Q. Unexpected Highly Reversible Topotactic CO_2 Sorption/Desorption Capacity for Potassium Dititanate. *J. Mater. Chem. A* **2016**, *4* (33), 12889–12896.
(9) Chigrin, P. G.; Kirichenko, E. A.; Rudnev, V. S.; Lukiyanchuk, I.; Yarovaya, T. P. Catalytic Properties of $K_2Ti_2O_5$ + $K_2Ti_4O_9$/TiO_2/TiO_2 + SiO_2/Ti Composites and Their Resistance to Environment Effects during the Process of Carbon Black Oxidation. *Prot. Met. Phys. Chem. Surf.* **2019**, *55* (1), 109–114.
(10) Federicci, R.; Holé, S.; Popa, A. F.; Brohan, L.; Baptiste, B.; Mercone, S.; Leridon, B. $Rb_2Ti_2O_5$:Superionic Conductor with Colossal Dielectric Constant. *Phys. Rev. Materials* **2017**, *1* (3), 032001.
(11) Rani, R.; De Sousa Coutinho, S.; Holé, S.; Leridon, B. Colossal Dielectric Constant in $K_2Ti_2O_5$. *Materials Letters* **2020**, *258*, 126784.
(12) Coutinho, S. D. S.; Federicci, R.; Hole, S.; Leridon, B. Virtual Cathode Induced in $Rb_2Ti_2O_5$ Solid Electrolyte. *Solid State Ion.* **2019**, *333*, 72–75.
(13) Coutinho, S. de S.; Berardan, D.; Lang, G.; Federicci, R.; Giura, P.; Beneut, K.; Dragoe, N.; Hole, S.; Leridon, B. Effect of Water Incorporation on the Ionic Conduction Properties of the Solid Electrolyte Material $Rb_2Ti_2O_5.(H_2O)_x$. *Solid State Ion.* **2021**, *364*, 115630.
(14) Chen, G.; Si, R.; Li, T.; Chen, P.; Wei, K.; Xie, X.; Chen, C.; Wang, C. Superior Linear Response of $K_2Ti_2O_5$ in Low and Medium Humidity Ranges. *ACS Appl. Electron. Mater.* **2021**, *3* (8), 3445–3450.
(15) Bamberger, C. E.; Begun, G. M.; MacDougall, C. S. Raman Spectroscopy of Potassium Titanates: Their Synthesis, Hydrolytic Reactions, and Thermal Stability. *Appl. Spectrosc., AS* **1990**, *44* (1), 30–37.
(16) Rodríguez-Carvajal, J. Recent Advances in Magnetic Structure Determination by Neutron Powder Diffraction. *Physica B: Condensed Matter* **1993**, *192* (1), 55–69.
(17) Lehman, R. L.; Gentry, J. S.; Glumac, N. G. Thermal Stability of Potassium Carbonate near Its Melting Point. *Thermochim. Acta* **1998**, *316* (1), 1–9.
(18) Liu, C.; Lu, X.; Yu, G.; Feng, X.; Zhang, Q.; Xu, Z. Role of an Intermediate Phase in Solid State Reaction of Hydrous Titanium Oxide with Potassium Carbonate. *Materials Chemistry and Physics* **2005**, *94* (2), 401–407.
(19) Bao, N.; Shen, L.; Feng, X.; Lu, X. High Quality and Yield in Potassium Titanate Whiskers Synthesized by Calcination from Hydrous Titania. *Journal of the American Ceramic Society* **2004**, *87* (3), 326–330.
(20) Abouelhassan, S.; Salman, F.; Elmansy, M.; Sheha, E. Characterization of $KhCO_3$ Single Crystals. *Surf. Rev. Lett.* **2004**, *11* (01), 83–86.

(21) Narvor, A. L.; Saumagne, P.; Novak, A. Étude par spectroscopie infrarouge des hydrogéno et deutériocarbonates de rubidium et de césium et des sesquicarbonates de potassium et de rubidium. *J. Chim. Phys.* **1967**, *64*, 1643–1648.
(22) Tatzber, M.; Stemmer, M.; Spiegel, H.; Katzlberger, C.; Haberhauer, G.; Gerzabek, M. H. An Alternative Method to Measure Carbonate in Soils by FT-IR Spectroscopy. *Environ Chem Lett* **2007**, *5* (1), 9–12.
(23) Novak, A.; Saumagne, P.; Bok, L. Étude par spectroscopie infrarouge de quelques hydrogénocarbonates alcalins: $NaHCO_3$, NH_4HCO_3 et $KHCO_3$ et du sesquicarbonate de sodium: Na_2CO_3 . $NaHCO_3$. $2H_2O$. *J. Chim. Phys.* **1963**, *60*, 1385–1395.
(24) Qi, X.; Pan, C. Synthesis of Nano-/Microsized $KHCO_3$ Fibers via Quick Thermal Process and Its Toughness and Electron-Irradiating Degradation. *J. Phys. Chem. C* **2009**, *113* (45), 19439–19444.
(25) Kang, S.; Singh, A.; Reeves, K. G.; Badot, J.-C.; Durand-Vidal, S.; Legein, C.; Body, M.; Dubrunfaut, O.; Borkiewicz, O. J.; Tremblay, B.; Laberty-Robert, C.; Dambournet, D. Hydronium Ions Stabilized in a Titanate-Layered Structure with High Ionic Conductivity: Application to Aqueous Proton Batteries. *Chem. Mater.* **2020**, *32* (21), 9458–9469.

Supporting Information

Chemical and structural evolution of $Rb_{2-2x}K_{2x}Ti_2O_5$ layered titanates when exposed to ambient air

Narimane Meziani[1], Méline Parent[2], Gwenaëlle Rousse[3], Brigitte Leridon[4], David Berardan[1],*, Paola Giura[2],*

[1] Institut de Chimie Moléculaire et des Matériaux d'Orsay, CNRS, Université Paris-Saclay, Orsay, France
[2] Institut de Minéralogie, de Physique des Matériaux et de Cosmochimie, Sorbonne Université, Paris, France
[3] Laboratoire de Chimie du Solide et Énergie, UMR 8260, Collège de France, Sorbonne Université, Paris, France
[4] Laboratoire de Physique et d'Etude des Matériaux, UMR8213 ESPCI Paris, PSL Université, CNRS, Sorbonne Université, Paris, France
* Corresponding authors : e-mail address: : david.berardan@u-psud.fr and paola.giura@sorbonne-universite.fr

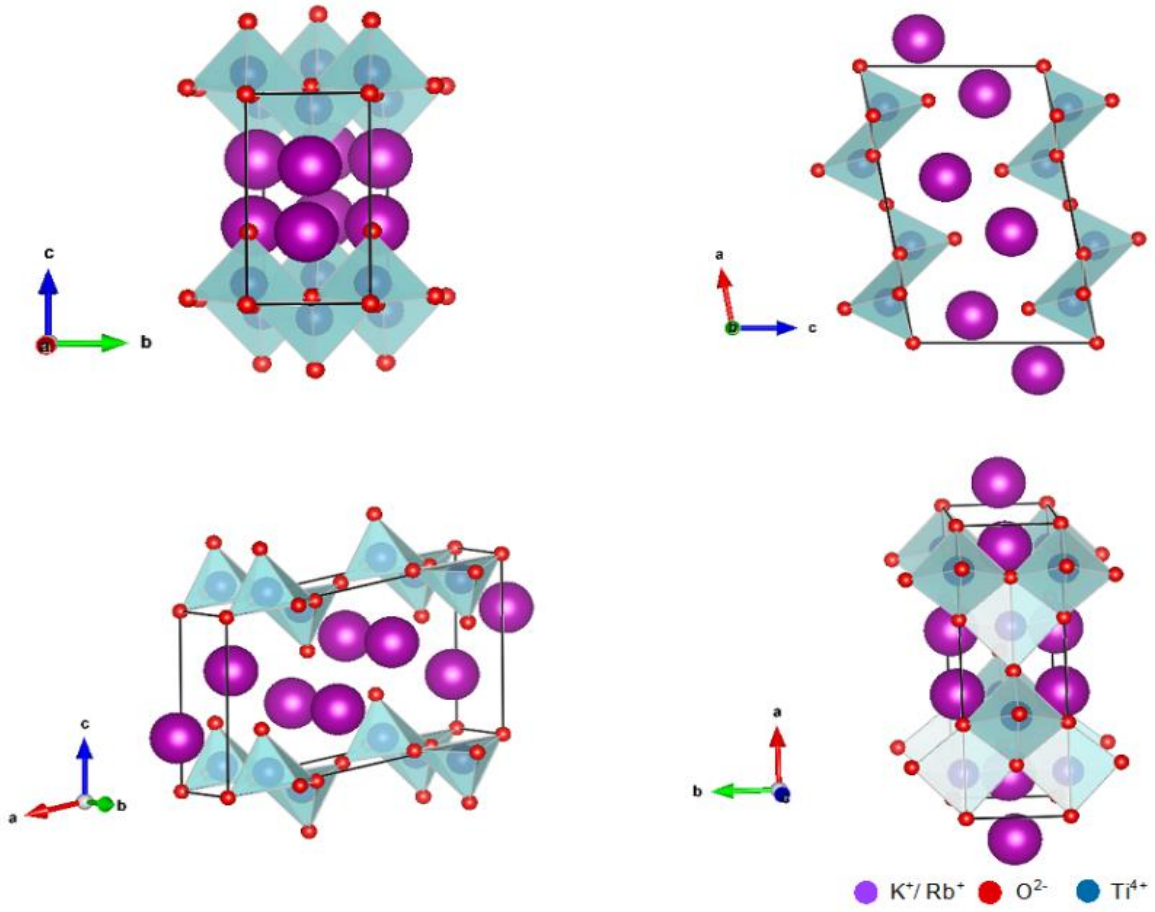

Figure S1: Crystal structure of $M_2Ti_2O_5$ represented upon different orientations. (Rb is shown as purple balls, O as red ones and Ti as blue-gray ones)

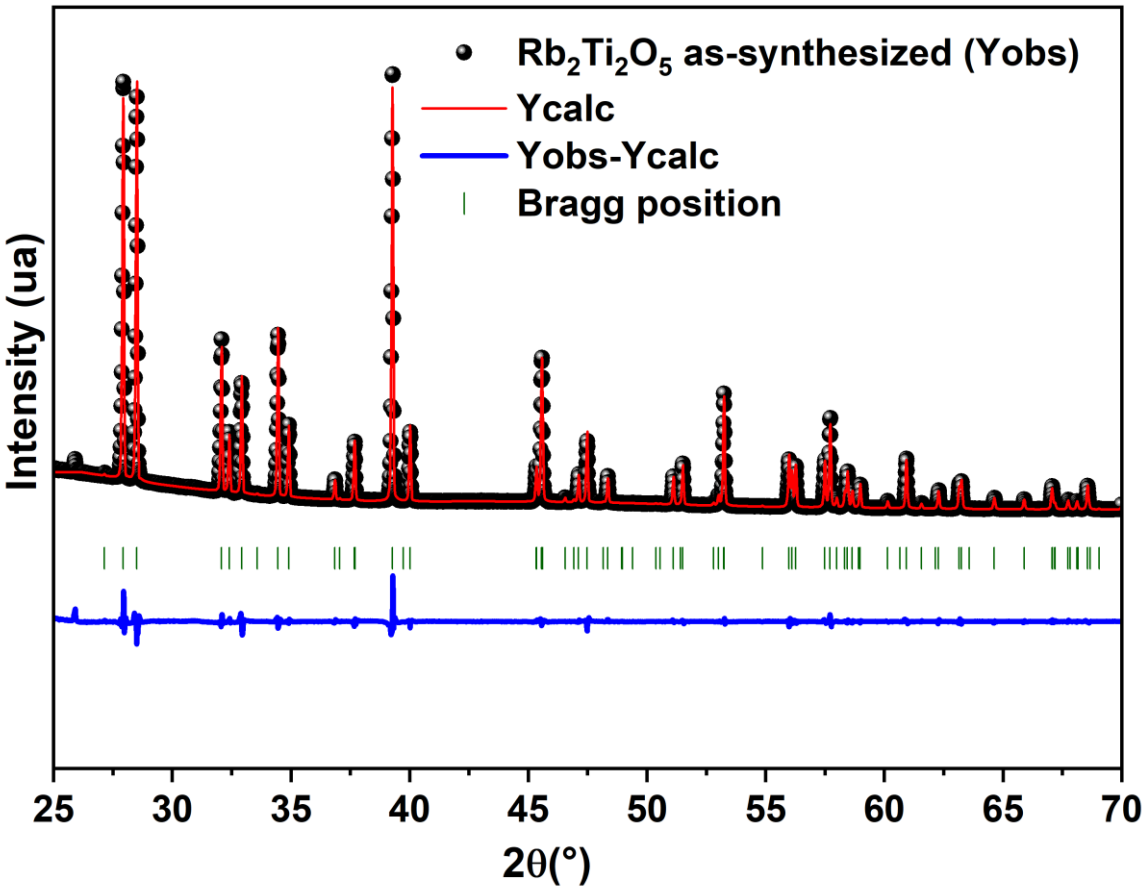

Figure S2: Le Bail refinement of $Rb_2Ti_2O_5$. Black circles, red line, blue line and vertical green tick marks represent the observed, calculated, difference pattern and Bragg positions, respectively.

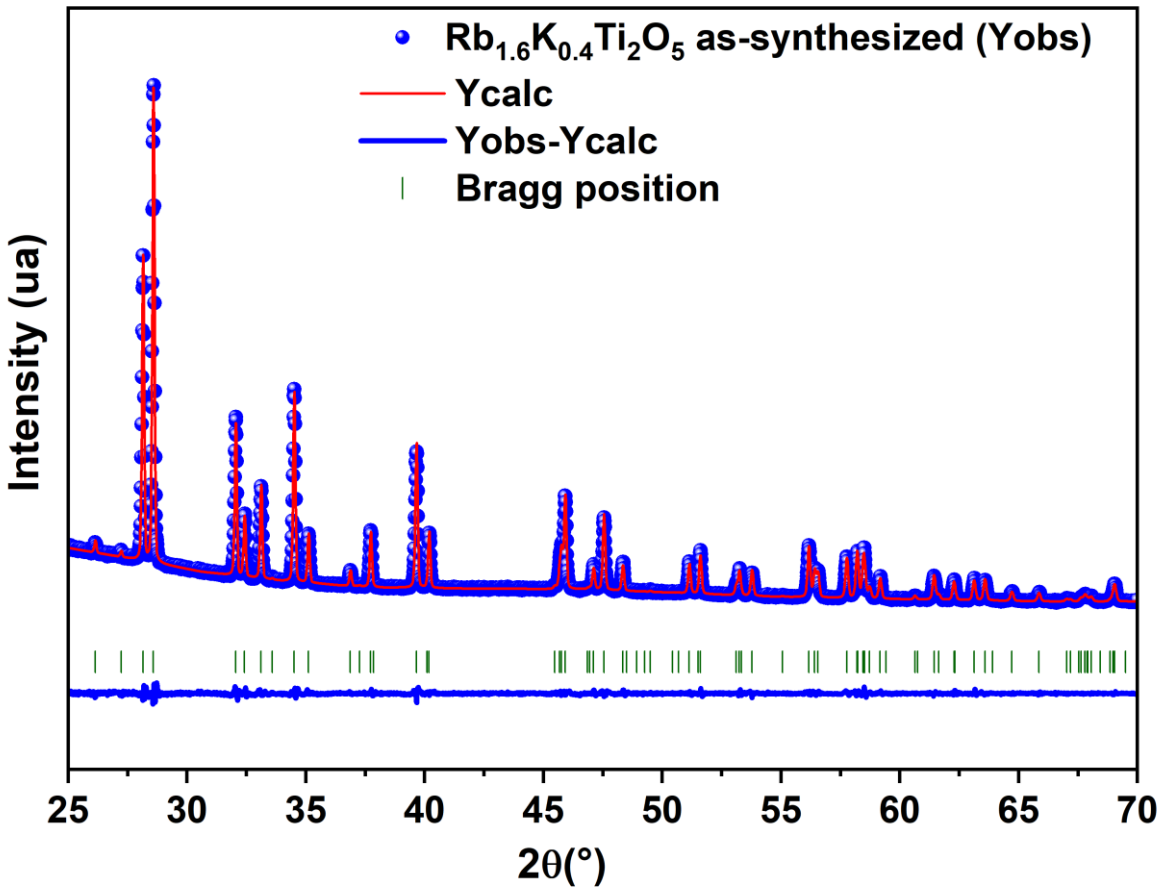

Figure S3: Le Bail refinement of $Rb_{1.6}K_{0.4}Ti_2O_5$. Blue circles, red line, blue line and vertical green tick marks represent the observed, calculated, difference pattern and Bragg positions, respectively.

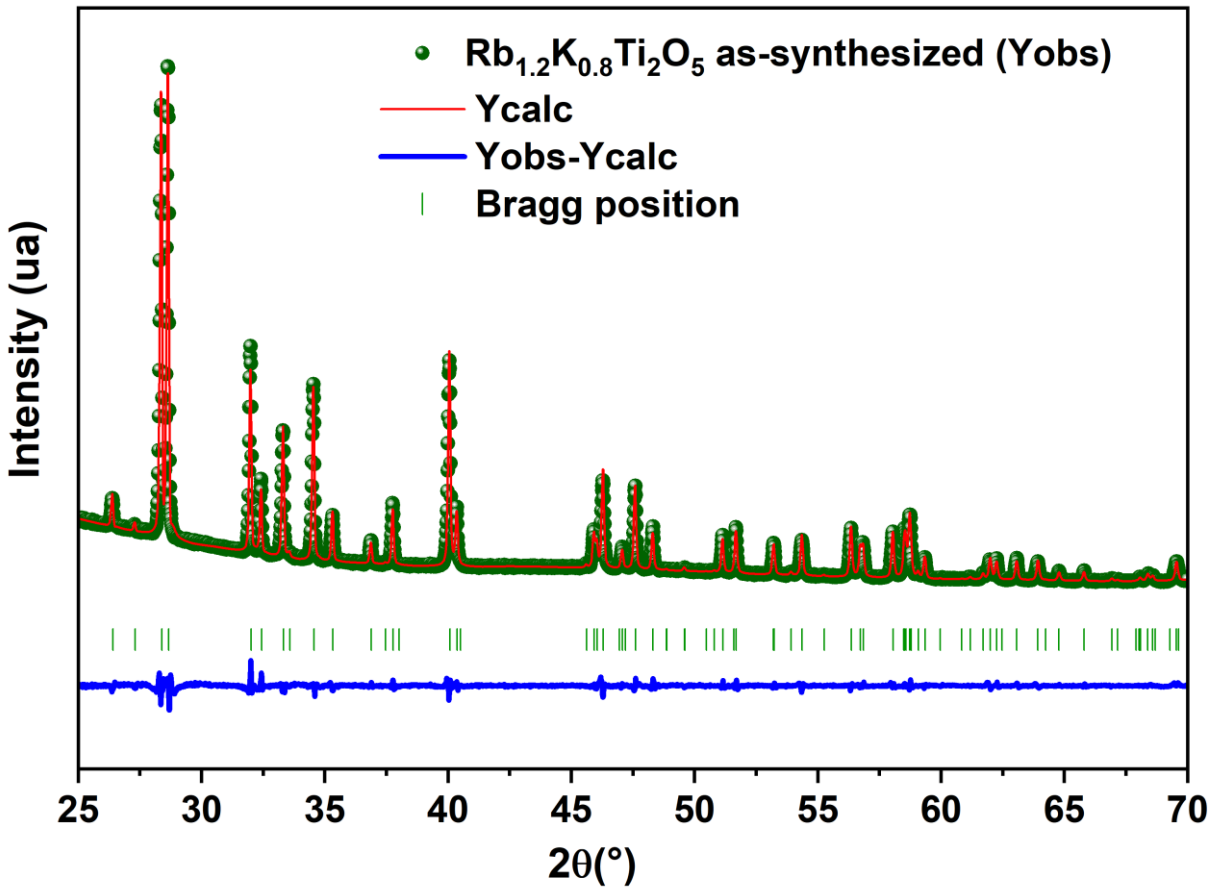

Figure S4: Le Bail refinement of $Rb_{1.2}K_{0.8}Ti_2O_5$. Olive circles, red line, blue line and vertical green tick marks represent the observed, calculated, difference pattern and Bragg positions, respectively.

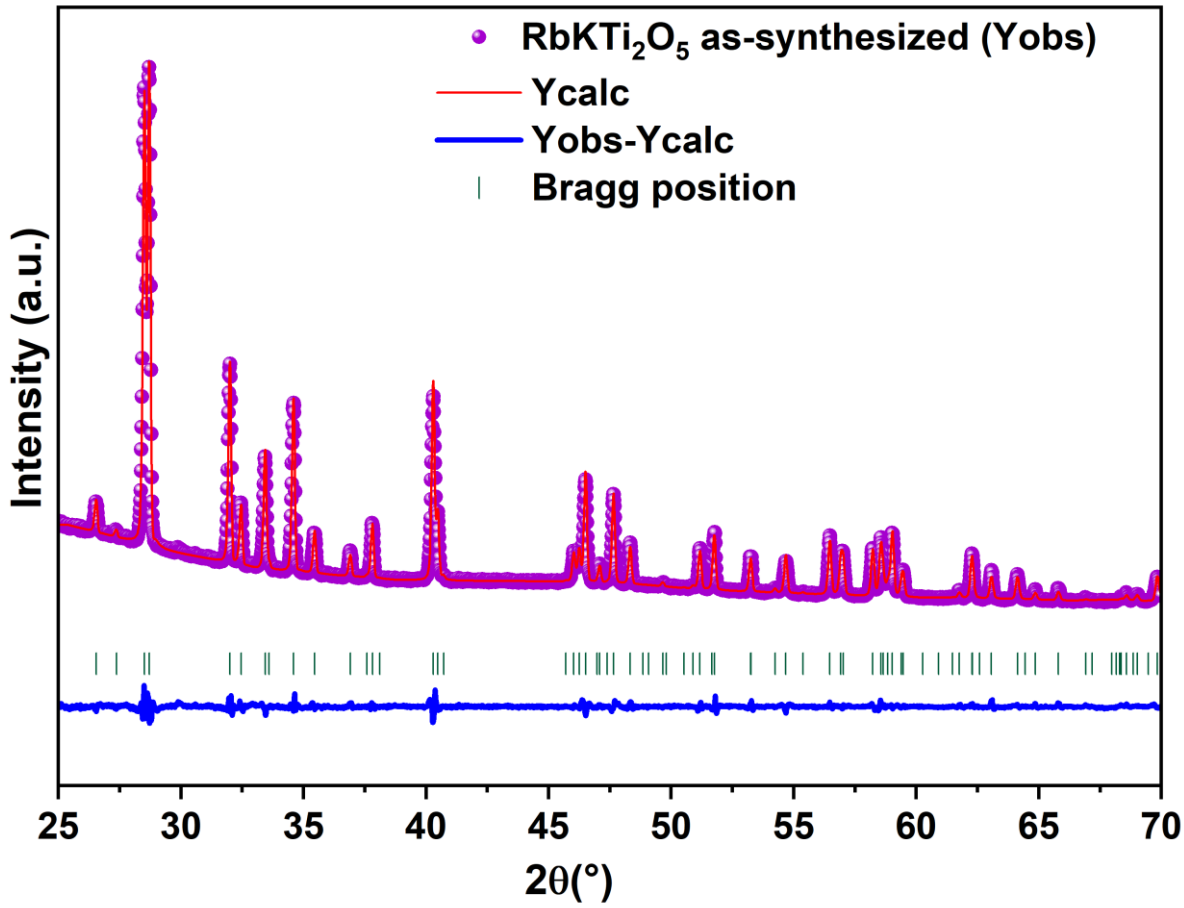

Figure S5: Le Bail refinement of $RbKTi_2O_5$. Purple circles, red line, blue line and vertical green tick marks represent the observed, calculated, difference pattern and Bragg positions, respectively.

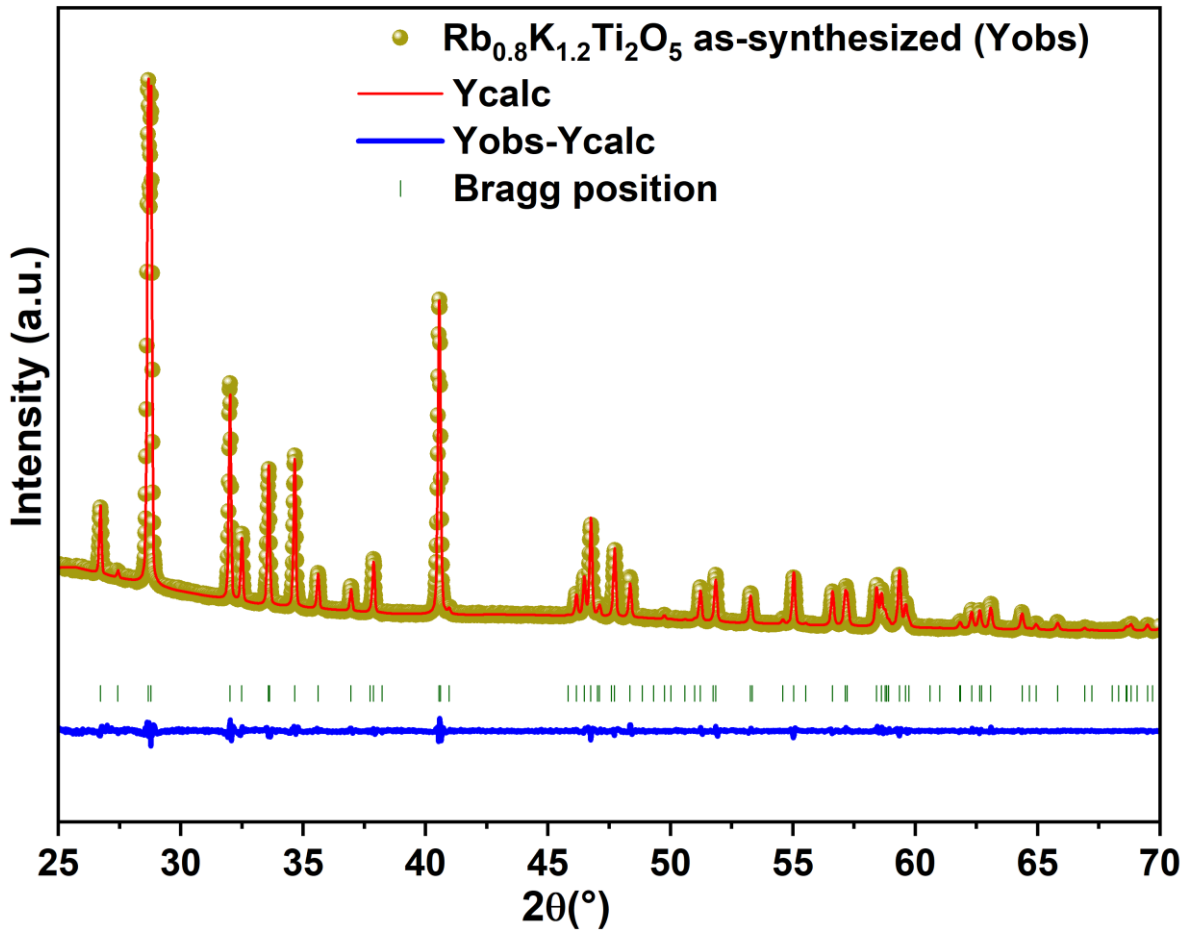

Figure S6: Le Bail refinement of $Rb_{0.8}K_{1.2}Ti_2O_5$. Dark yellow circles, red line, blue line and vertical green tick marks represent the observed, calculated, difference pattern and Bragg positions, respectively.

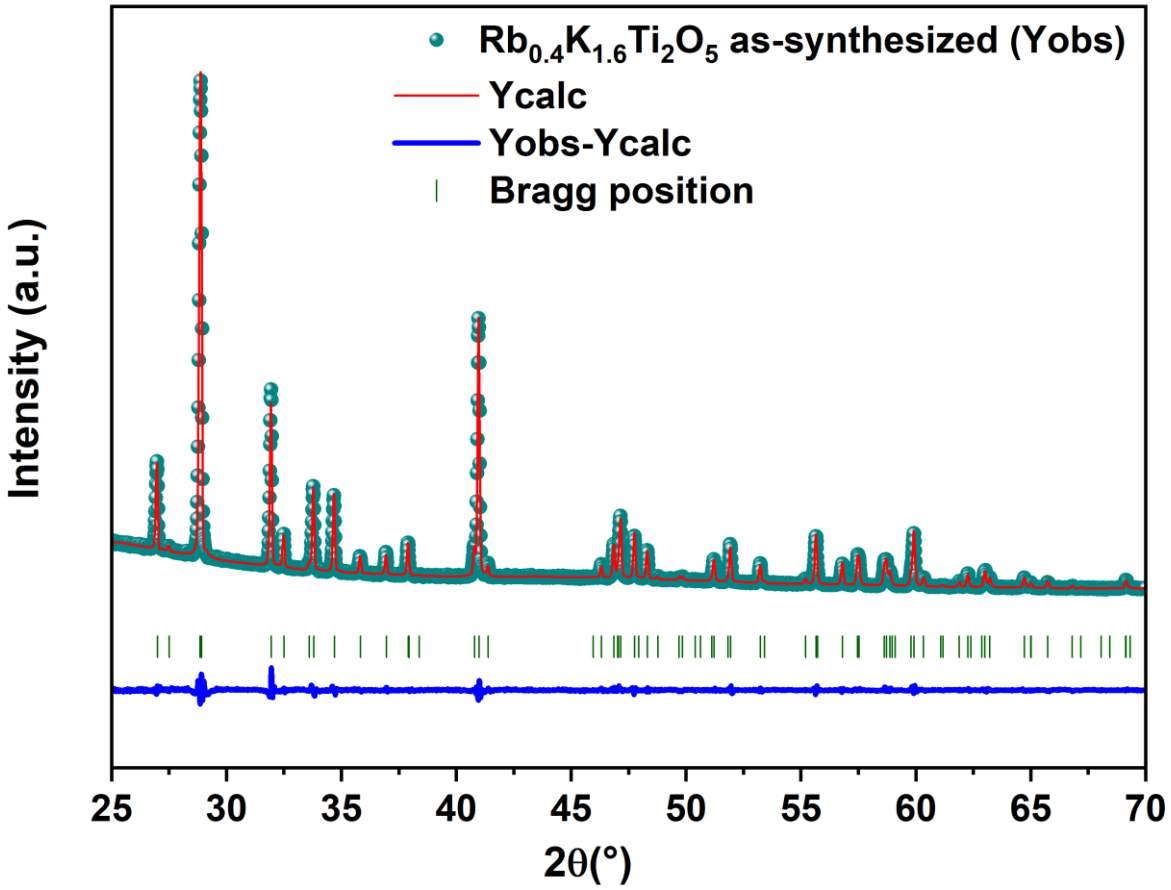

Figure S7: Le Bail refinement of $Rb_{0.4}K_{1.6}Ti_2O_5$. Dark cyan circles, red line, blue line and vertical green tick marks represent the observed, calculated, difference pattern and Bragg positions, respectively.

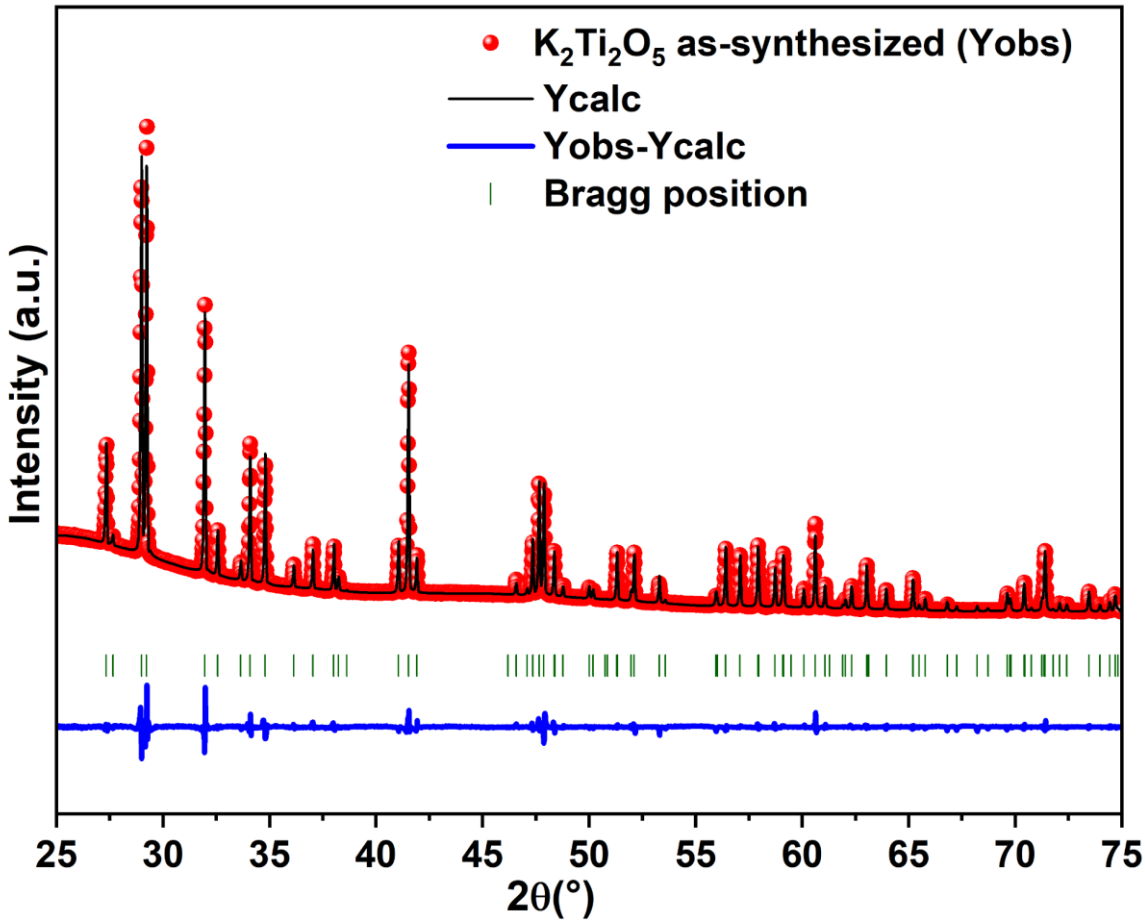

Figure S8: Le Bail refinement of $K_2Ti_2O_5$. Red circles, dark line, blue line and vertical green tick marks represent the observed, calculated, difference pattern and Bragg positions, respectively.

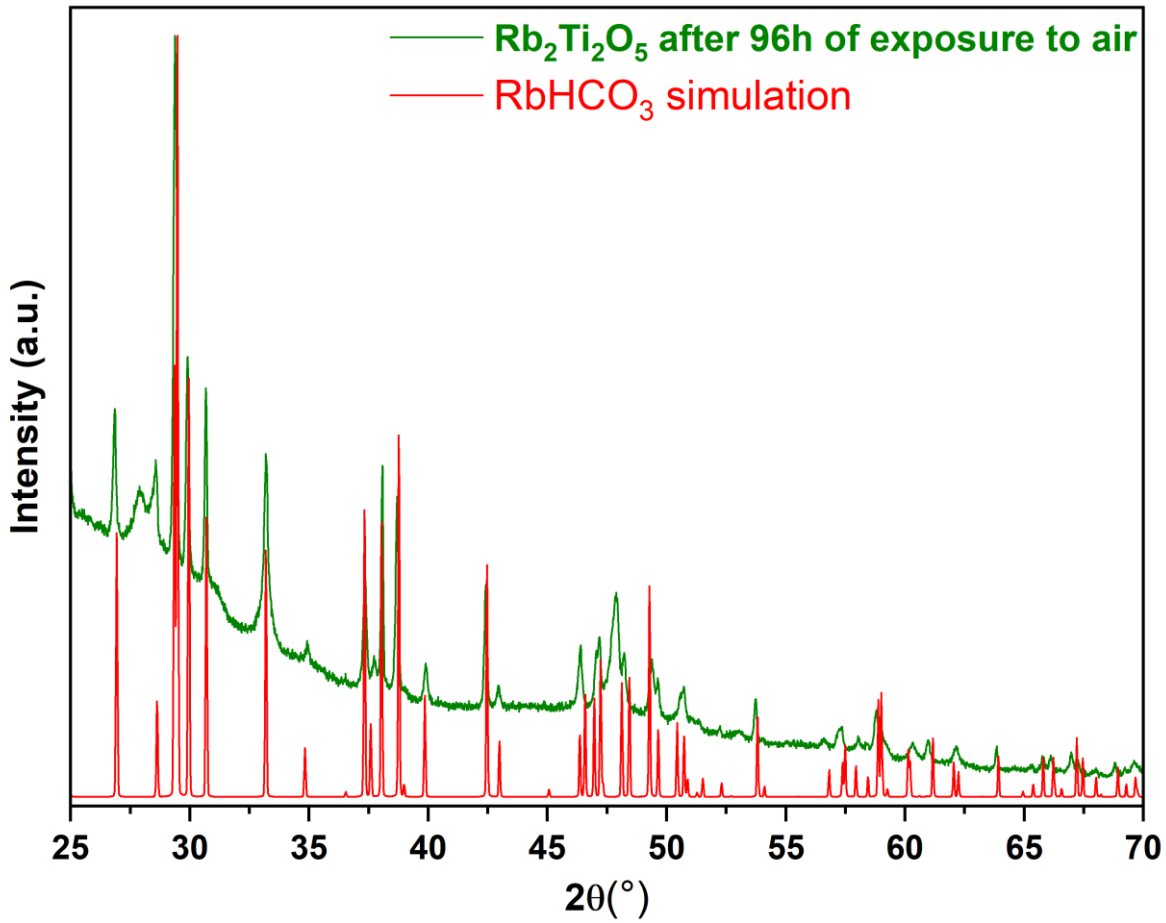

Figure S9 Overlay of the diffractogram of $Rb_2Ti_2O_5$ exposed to air for 96 hours with that of the simulated $RBHCO_3$ in red curve.

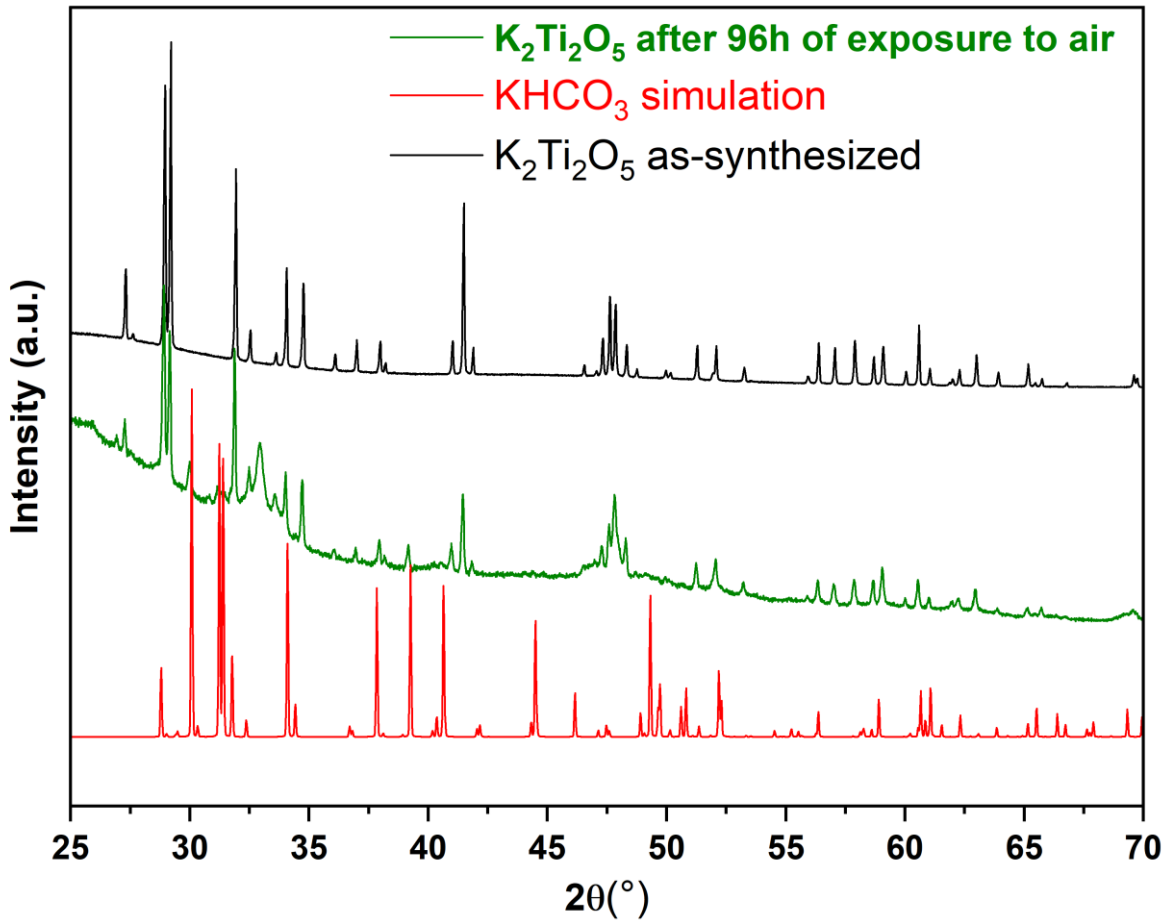

Figure S10 : Overlay of the diffractogram of $K_2Ti_2O_5$ as-synthesized and exposed to air for 96 hours with that of the simulated $KHCO_3$ in red curve.

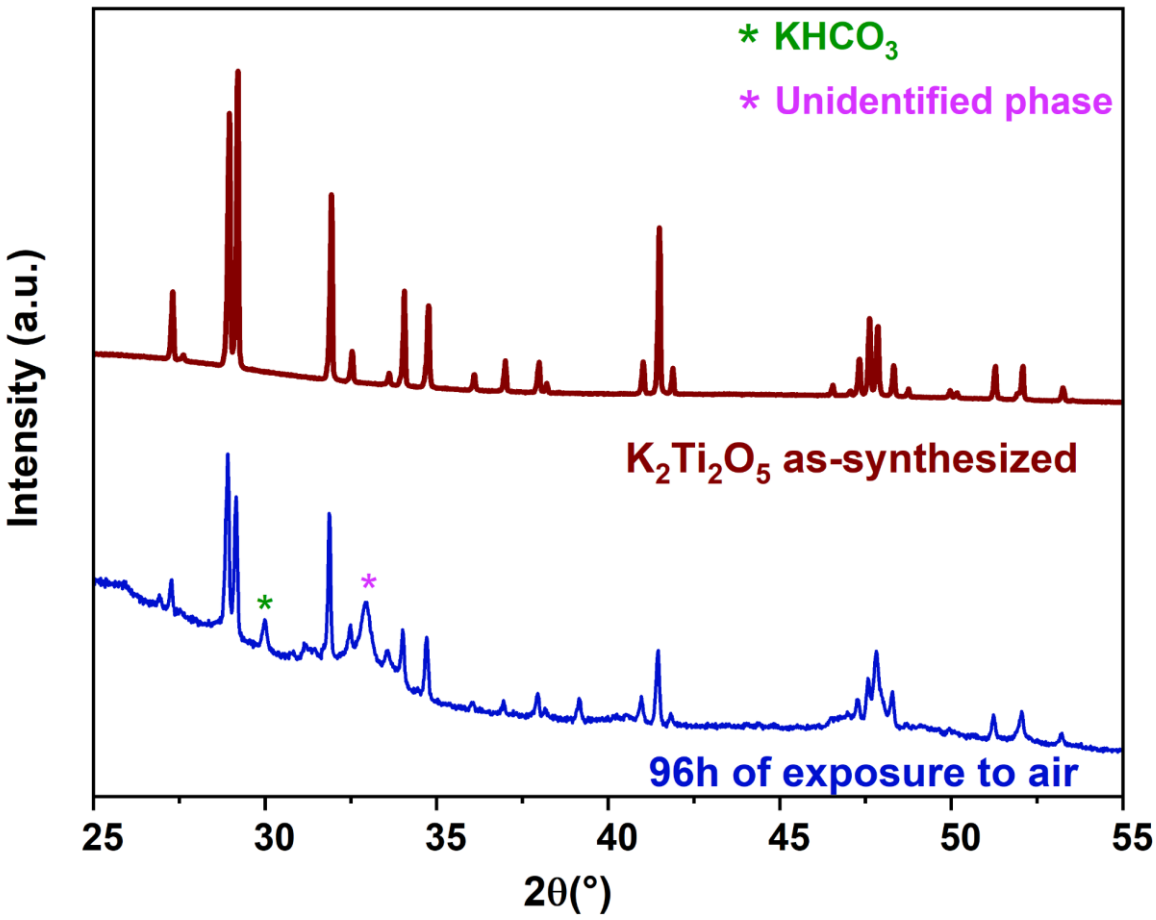

Figure S11: XRD pattern of $K_2Ti_2O_5$, as synthesized and after 96h of exposure to ambient air.

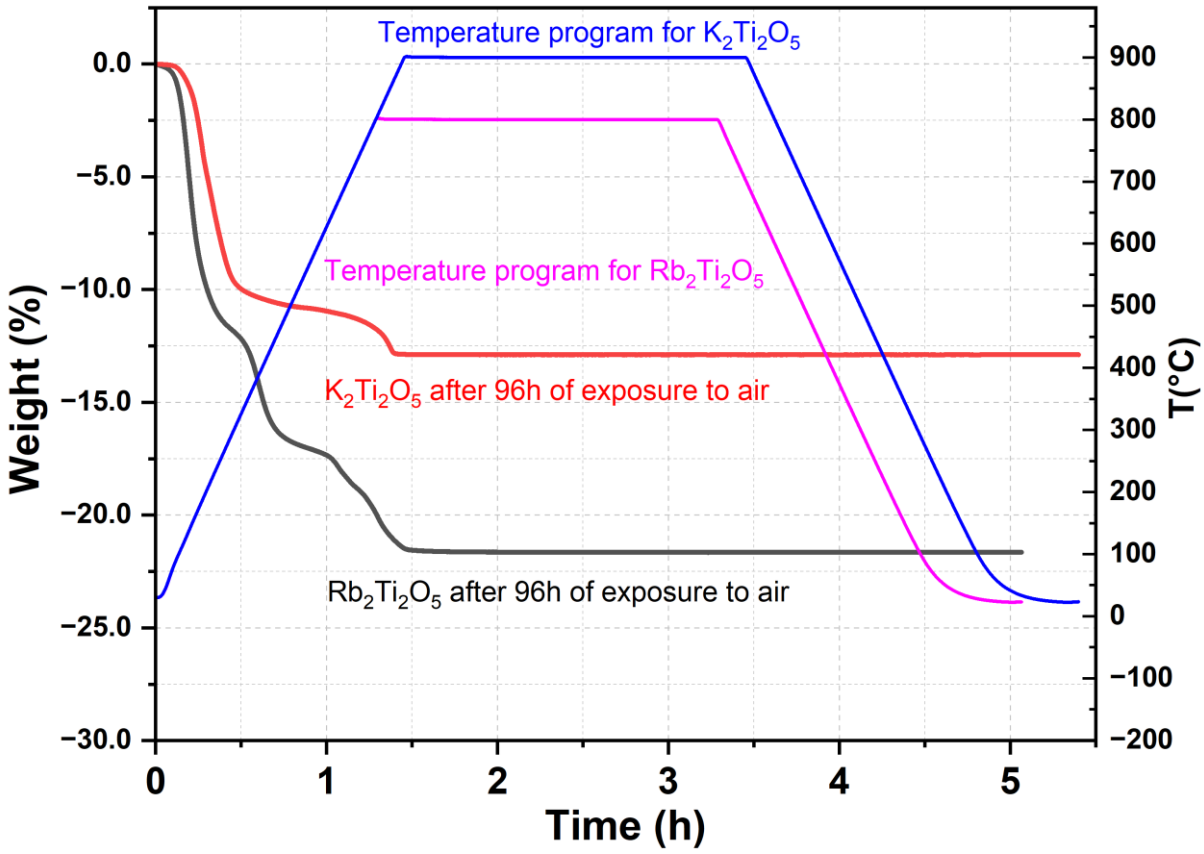

Figure S12: Representative example of the raw data of some thermogravimetric analyses, showing the weight loss ends during the high-temperature plateau.

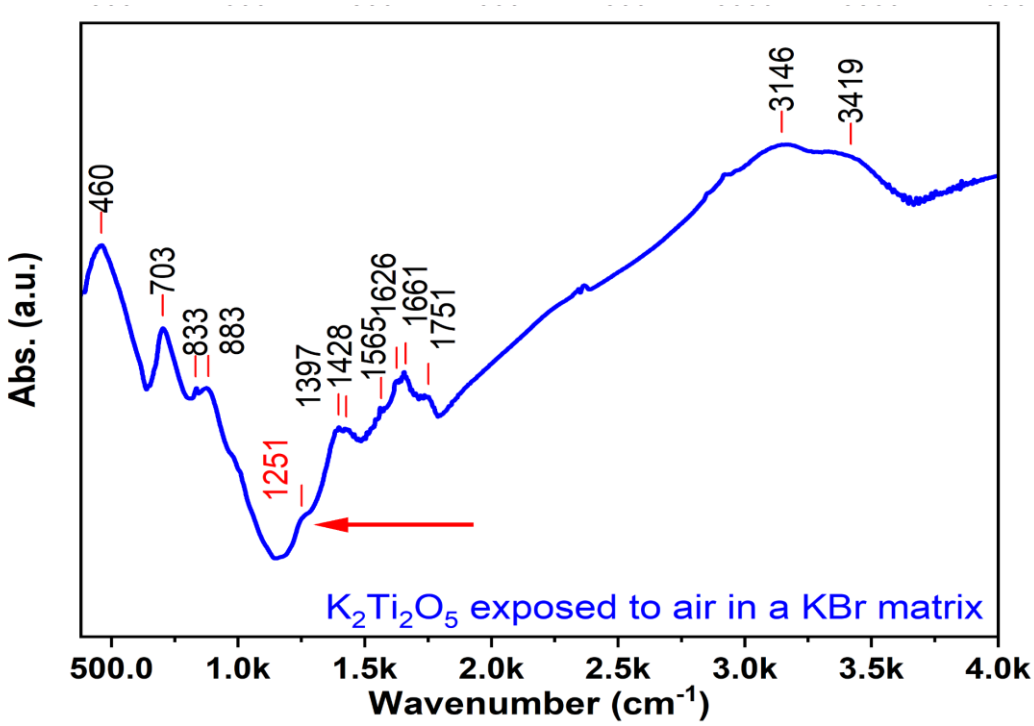

Figure S13: IR spectrum of $K_2Ti_2O_5$ exposed to ambient air within a KBr matrix.

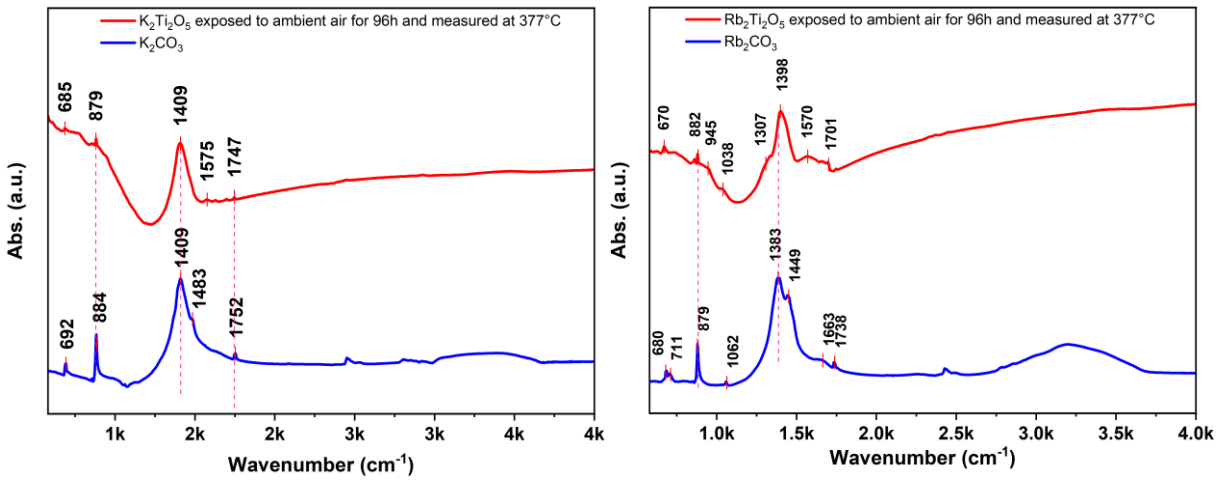

Figure S14: IR of $Rb_2Ti_2O_5$ and $K_2Ti_2O_2$ exposed to ambient air during 96h and measured above the dehydration temperature, as compared to IR spectra of Rb_2CO_3 and K_2CO_3

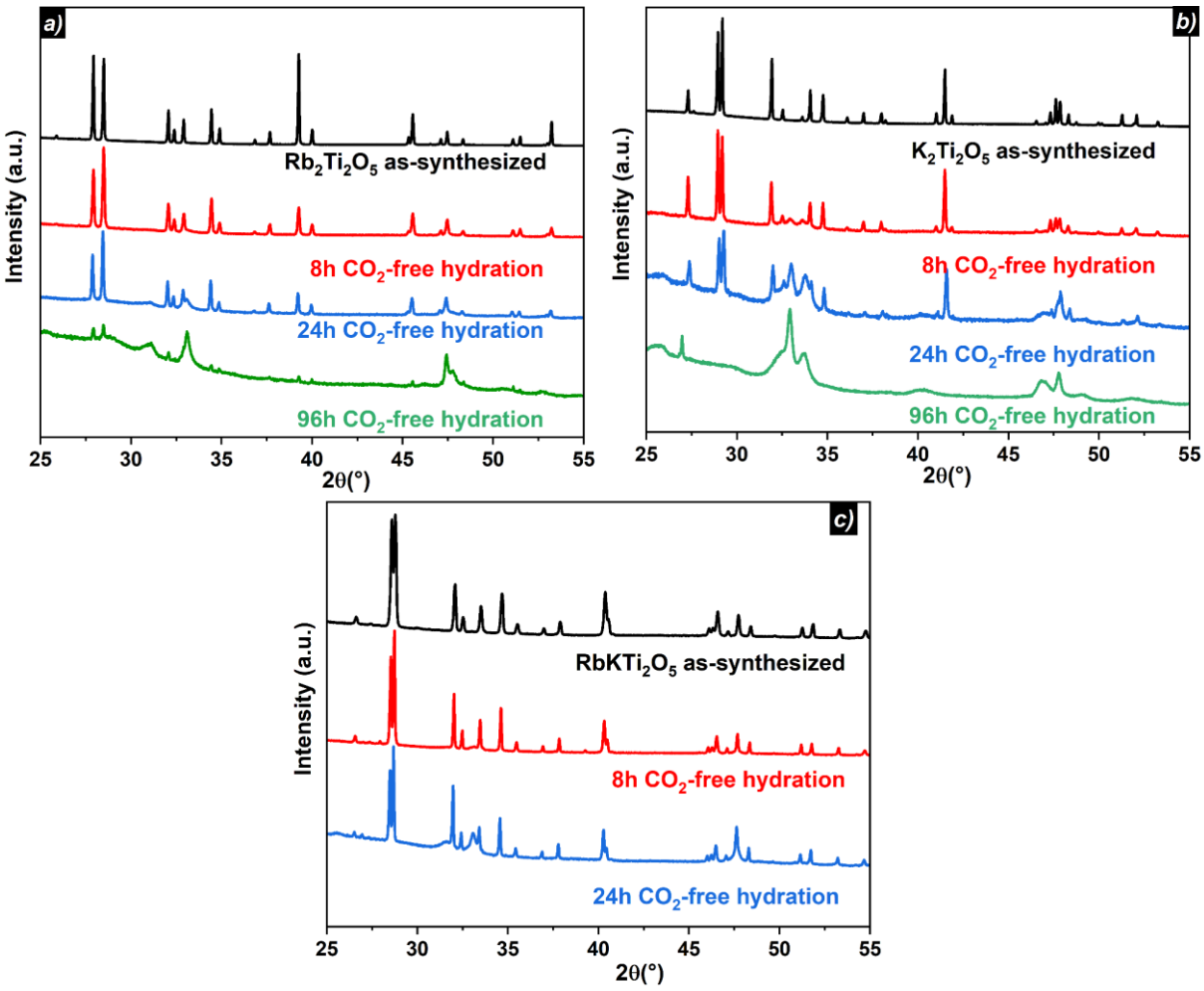

Figure S15: (a) XRD patterns of $Rb_2Ti_2O_5$, as-synthesized and after hydration in a CO_2-free environment. (b) XRD patterns of $K_2Ti_2O_5$, as-synthesized and after hydration in a CO_2-free environment. (c) XRD patterns of $RbKTi_2O_5$, as-synthesized and after hydration in a CO_2-free environment. Note that some changes of the relative intensities of the (2 0 2) and (1 1 1) peaks located around 2θ=28-29° can occur from one sample to another due to differences of preferential orientation of the crystallites during XRD analysis. These differences should be considered as artefacts.

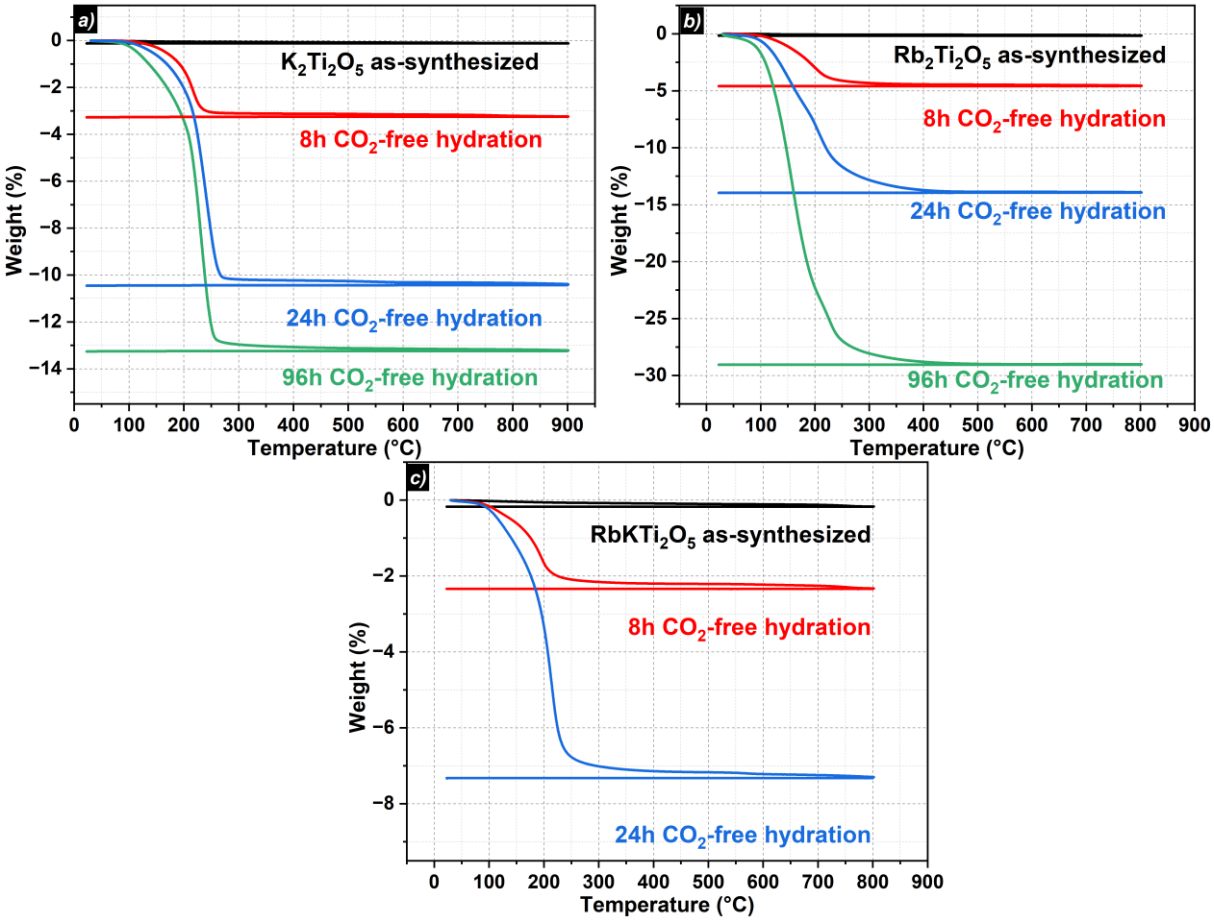

Figure S16: TGA analysis of $M_2Ti_2O_5$ samples, as synthesized and hydrated in a CO_2-free environment. (a) $K_2Ti_2O_5$, (b) $Rb_2Ti_2O_5$, (c) $RbKTi_2O_5$. Note that the y-scale is not the same for all figures.

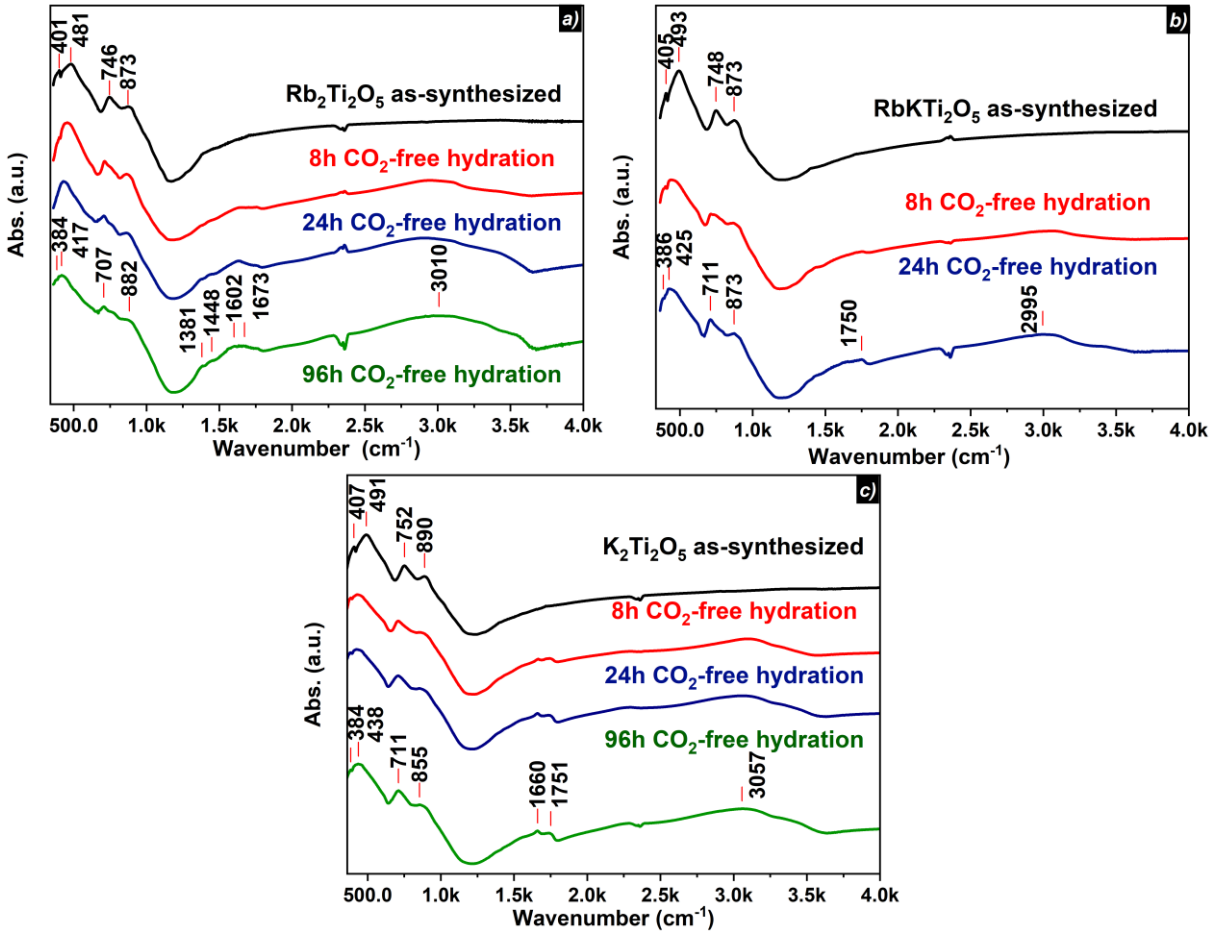

Figure S17: Room temperature IR spectra of $M_2Ti_2O_5$, as synthesized and after hydration in a CO_2-free environment. (a) $Rb_2Ti_2O_5$, (b) $RbKTi_2O_5$ and (c) $K_2Ti_2O_5$.

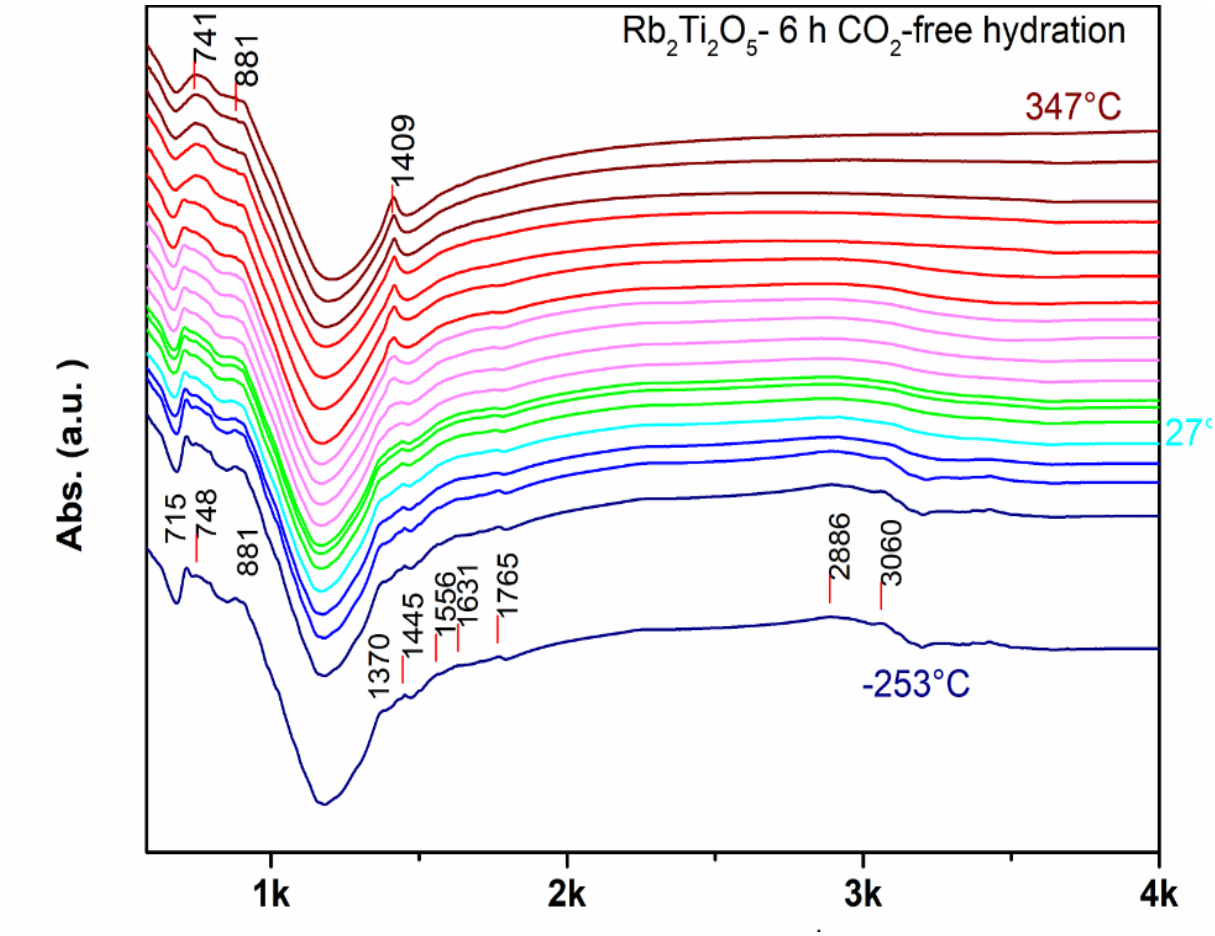

Figure S18: Temperature-dependent IR spectra of $Rb_2Ti_2O_5$ hydrated during 6h in a CO_2-free environment.

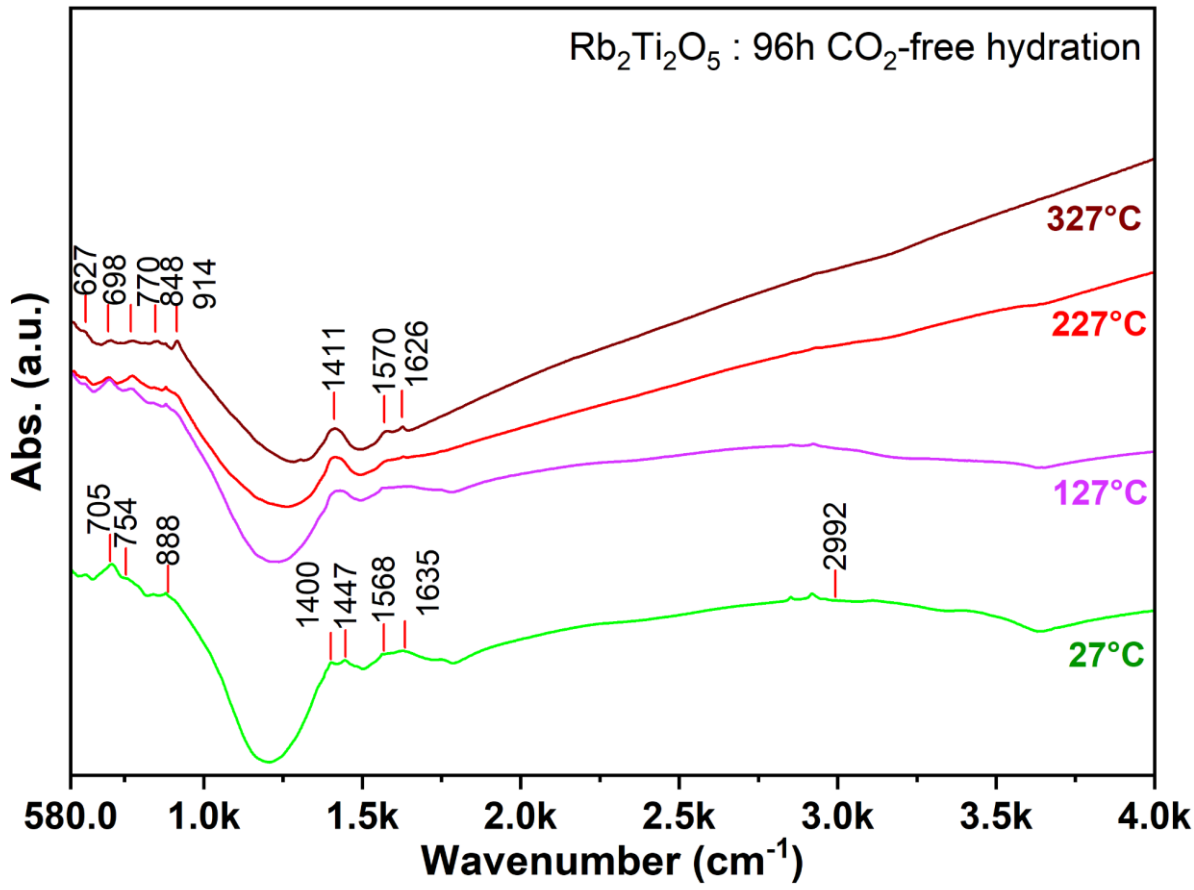

Figure S19: Temperature-dependent IR spectra of $Rb_2Ti_2O_5$ hydrated during 96h in a CO_2-free environment

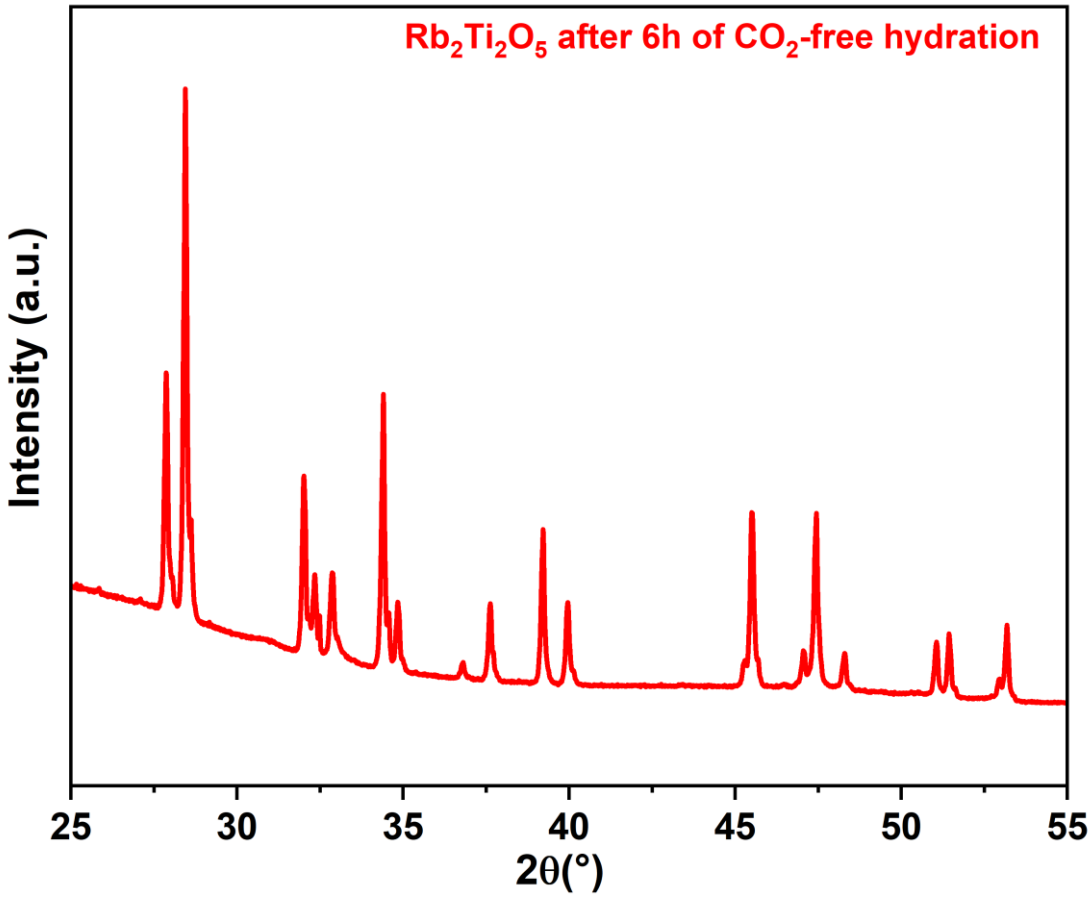

Figure S20: XRD pattern of $Rb_2Ti_2O_5$ hydrated in a CO_2-free environment during 6h

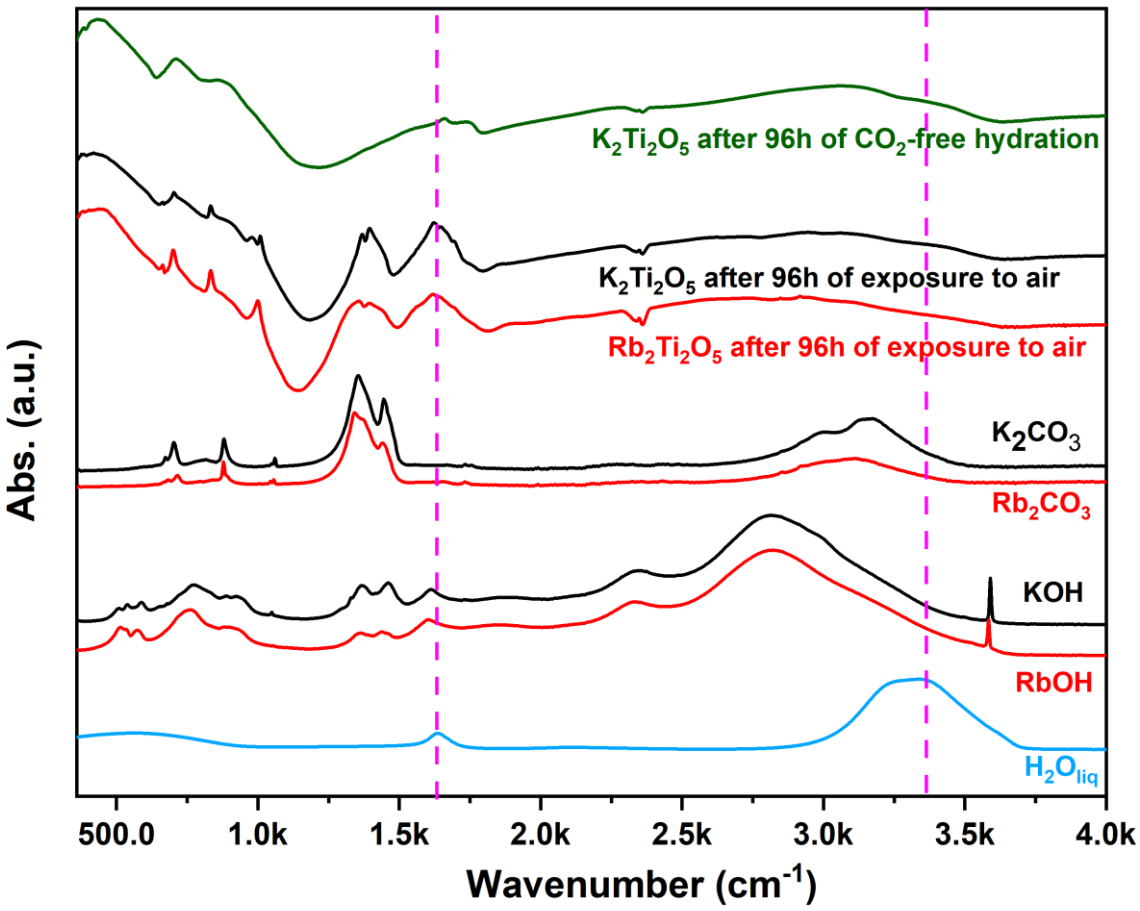

Figure S21: The room temperature comparison of IR spectra includes the following samples: $K_2Ti_2O_5$ after 96 hours of CO_2-free hydration (in green), $K_2Ti_2O_5$ (in black) and $Rb_2Ti_2O_5$ (in red) exposed to air for 96 hours, K_2CO_3 (in black) and Rb_2CO_3 (in red), KOH (in black) and RbOH (in red), as well as liquid water.

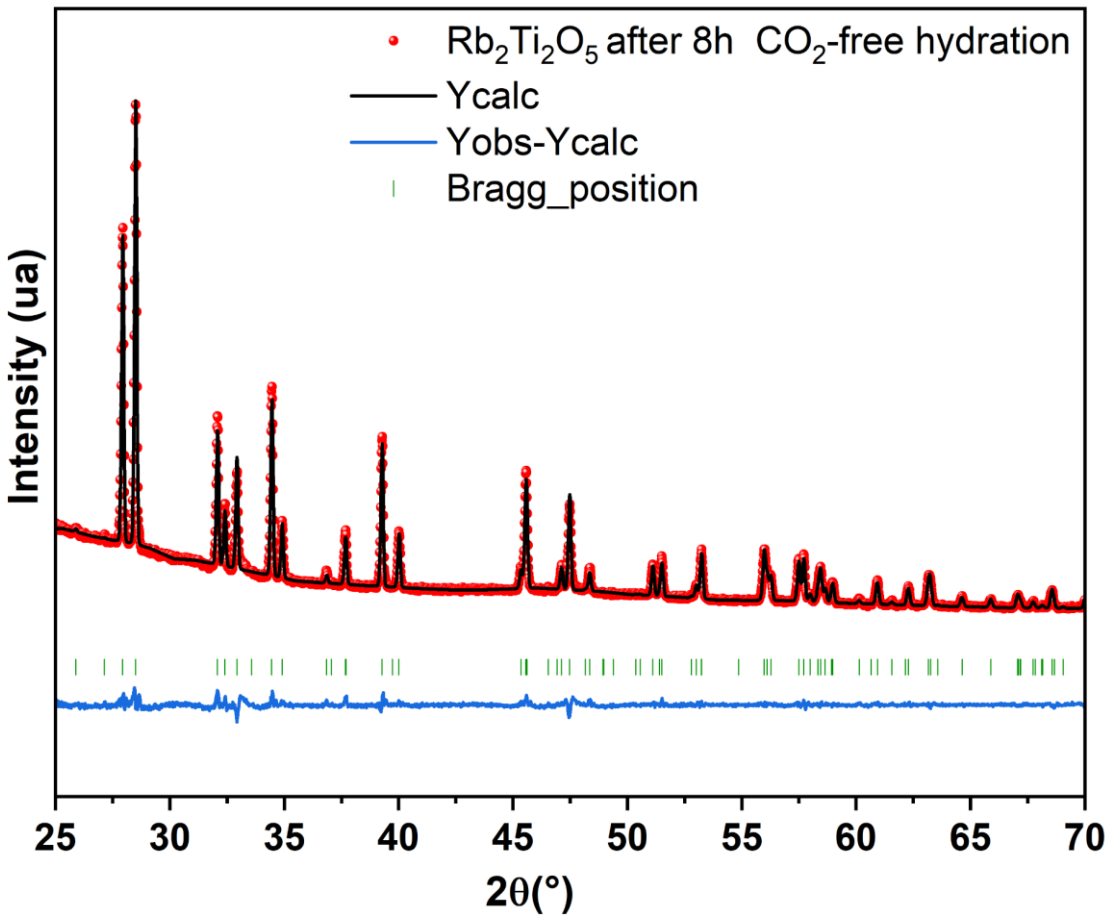

Figure S22: Le Bail refinement of the XRD pattern of $Rb_2Ti_2O_5$ hydrated in a CO_2-free environment during 8h. Red circles, dark line, blue line and vertical green tick marks represent the observed, calculated, difference pattern and Bragg positions, respectively.

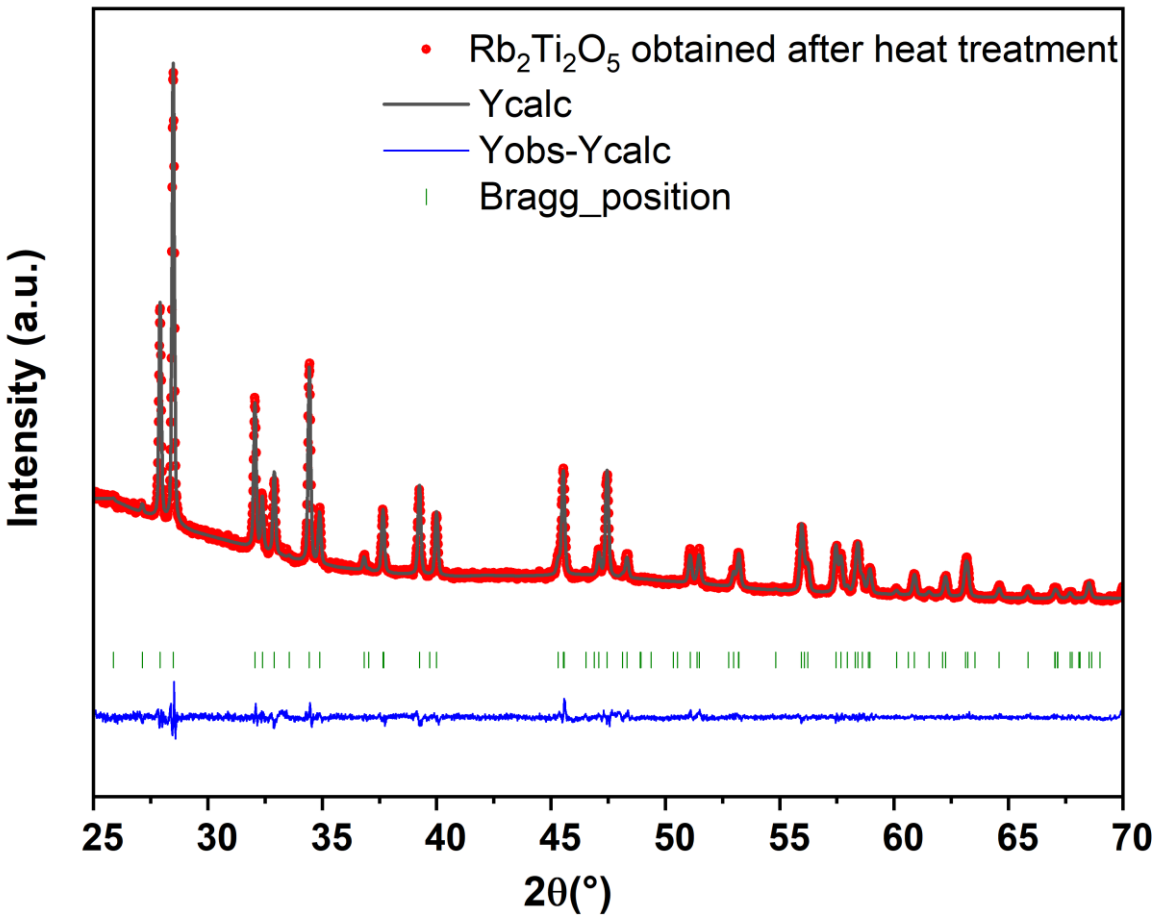

Figure S23: Le Bail refinement of the XRD pattern of a $Rb_2Ti_2O_5$ sample after 14 days of exposure to ambient air followed by a heat treatment of 1 hour at 800°C. Red circles, dark line, blue line and vertical green tick marks represent the observed, calculated, difference pattern and Bragg positions, respectively.

$Rb_2Ti_2O_5$	*a* (Å)	*b* (Å)	*c* (Å)	β (°)	Lattice volume (Å^3)
as-synthesized	11.333(2)	3.826(1)	6.990(1)	100.271(10)	298.28(10)
exposed to ambient air 14 days followed by a treatment of 1h at 800°C	11.340(2)	3.829(1)	6.992(1)	100.269(10)	298.78(10)
$Rb_2Ti_2O_5$ after 8h of CO_2-free hydration	11.335(2)	3.827(1)	6.989(1)	100.274(10)	298.36(10)

Table S1: evolution of the lattice parameters of the $Rb_2Ti_2O_5$ phase during degradation in ambient air or during hydration in a CO_2-free environment obtained from the Le Bail refinements shown in Figures S2, S22 and S23.